Identification of a Rubredoxin-like Protein Required for Biotin Synthesis in Mycobacteria

A THESIS TO THE GRADUATE DIVISION OF THE UNIVERSITY OF HAWAI'I AT MĀNOA IN PARTIAL FULFILLMENT OF THE REQUIREMENTS FOR THE DEGREE

OF

MASTER OF SCIENCE

IN

CHEMISTRY

December 2022

BY

KENNETH OMOLO

THESIS COMMITTEE:

Joseph Jarrett, Committee Chair

Ellinor Haglund

Rui Sun

ABSTRACT

In *Mycobacterium tuberculosis* (TB), biotin is crucial for synthesizing glucose, fatty acids, and mycolic acid components of the bacterial cell wall essential for survival and pathogenesis. TB grows in a biotin-deficient environment during infection and must synthesize its own biotin *de novo*. Biotin synthase catalyzes the final step in biotin synthesis, in which *S*-adenosylmethionine (SAM) is used to oxidize C-H bonds and a sulfur atom from an iron-sulfur cluster is inserted between two carbon atoms in the biotin precursor, dethiobiotin. In *E. coli*, biotin synthase also requires the exogenous electron donor flavodoxin, but this protein will not support the activity of the TB enzyme. In mycobacterial genomes, the biotin synthase gene (BioB or Rv1589 in TB) is found adjacent to two uncharacterized genes that code for small proteins with unknown functions (Rv1590 and Rv1591 in TB). Rv1590 codes for a metal-binding protein homologous to rubredoxin domains, suggesting Rv1590 could be involved in electron transfer reactions. This research project focuses on cloning the Rv1590 gene, heterologous expression in *E. coli*, purification of the resulting metalloprotein, and investigation of the secondary structure, thermal stability, metal content, and redox activity of the purified protein.

ACKNOWLEDGEMENTS

I would like to thank my supervisor Prof. Joseph Jarrett for allowing me to conduct this research in his lab and for his guidance and support throughout this project. I thank Dr. Haglund and her lab members for allowing me to use their lab equipment. Special thanks to my friends and family for their unwavering support and encouragement.

TABLE OF CONTENT

CHAPTER 1: INTRODUCTION

Mycobacterium Tuberculosis

Tuberculosis (TB) is an infectious disease caused by *Mycobacterium tuberculosis*, and it was the second major cause of death from an infectious disease in 2020, with a mortality of 1.5 million people. The bacterium is transmitted by tiny aerosol droplets mainly infecting the lungs, but it can also affect other organs, including the kidneys, the spine, and the brain (Shiloh, 2016). Tuberculosis drugs acts by inhibiting various biochemical processes in the bacterium, including protein synthesis, cell wall synthesis and nucleic acid synthesis. The dormant bacterium has evolved mechanisms to evade antibiotic treatment and patient's immune system to be reactivated once treatment has stopped or the immune system is weakened. Some bacteria strains are resistant to the first-line drugs, isoniazid, and rifampin, while others are resistant to less commonly used drugs such as fluoroquinolone and injectable second-line drugs (i.e., amikacin, kanamycin, or capreomycin) (Günther, 2014). The complex life cycle of the bacterium and the rising number of drug-resistant strains pose major challenges in TB treatment. New drugs are needed in the fight to eradicate TB. A common strategy in antibiotic drug discovery is targeting the metabolic pathways essential for bacterium survival and pathogenicity.

The Role of Biotin in *Mycobacterium tuberculosis*

Many organisms require biotin as a cofactor in carboxylation, decarboxylation, and transcarboxylation reactions essential for fatty acid biosynthesis, amino acid metabolism, and gluconeogenesis (Roth, 1981). Two ubiquitous enzymes that rely on biotin to transfer a carboxyl group onto their substrates are acetyl CoA carboxylase (ACC) and pyruvate carboxylase (PC) (Tong, 2013). The committed step in fatty acid biosynthesis is catalyzed by ACC in two consecutive reactions. The first reaction, catalyzed by the biotin carboxylase subunit of ACC, involves the activation of bicarbonate by ATP and the subsequent transfer of CO_2 onto a nitrogen atom on biotin. In the second reaction, catalyzed by the transcarboxylase subunit, the activated CO_2 is transferred from biotin to acetyl CoA to form malonyl CoA (Ohlrogge & Browse, 1995). Malonyl CoA is the essential precursor for the biosynthesis of both normal fatty acids found in membrane lipids and mycolic acids, which form the major component of the complex lipids of the mycobacterial thick outer cell membrane (Barry et al., 1998). The thick bacterial cell membrane enhances the mycobacteria's ability to resist chemical assault and limits its susceptibility to certain antibiotics (Ferguson & Rhoads, 2009). Pyruvate carboxylase relies on biotin as a cofactor in the fixation of CO_2 onto pyruvate to form oxaloacetate. Oxaloacetate is an important intermediate used to replenish the tricarboxylic acid cycle and to generate carbohydrates under nutrient limiting conditions (Jitrapakdee et al.,2008). The importance of biotin in these reactions makes the biotin biosynthetic pathway a promising target for developing new antimycobacterial drugs.

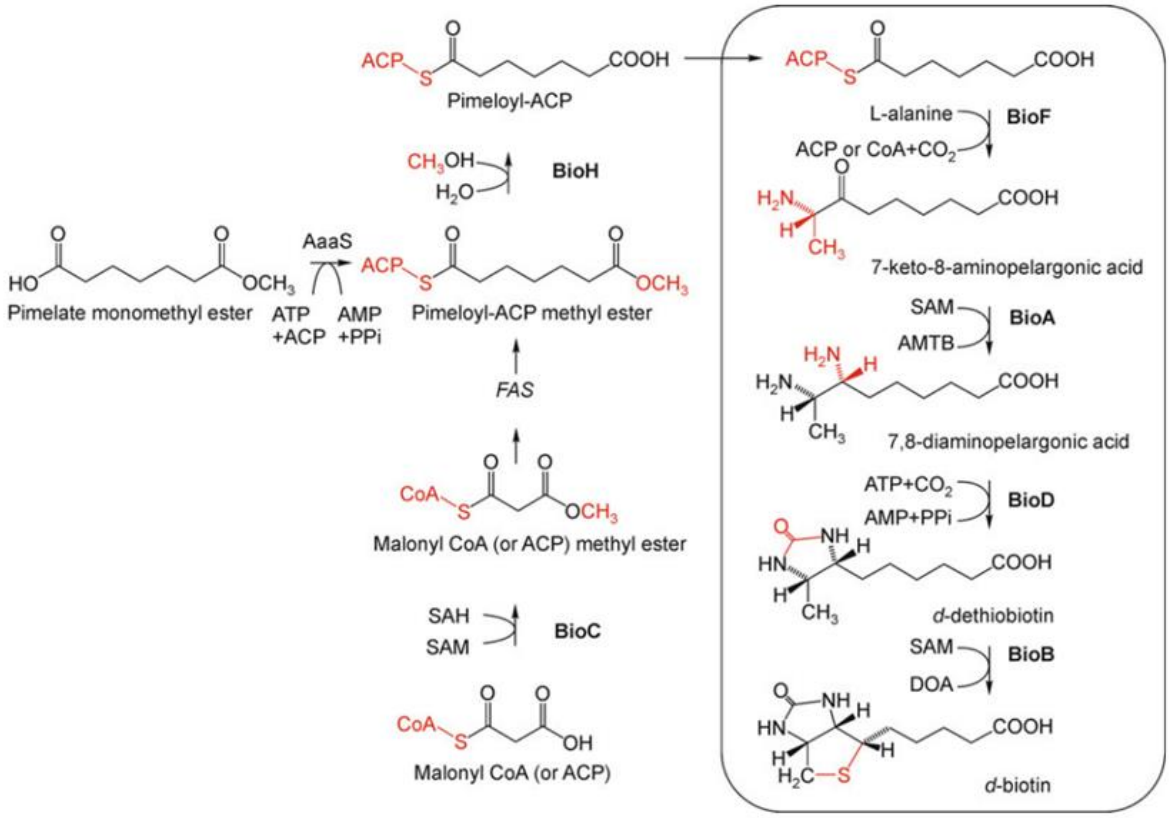

Figure 1. Biotin biosynthetic pathway in *E.coli*. The conserved reactions are boxed, and the non-conserved reactions are outside the box (Salaemae et al., 2011).

Biotin Biosynthetic Pathway

Although biotin is essential for all organisms, only plants, microorganisms, and some fungi can synthesize biotin (Cronan & Lin, 2011). Mammals have no biological pathways dedicated to biotin biosynthesis and depend on exogenous supply from the diet and the intestinal gut bacteria (Said, 2009). Some bacteria have transporters for uptaking exogenous biotin, such as the ATP-dependent biotin transporter, BioY (Finkenwirth et al., 2013), and YigM transporter in *E.coli* (Ludwig Ringlstetter, 2010). Genome annotation

studies of the *M. tuberculosis* genome have failed to identify homologs of BioY and YigM transporters (Hebbeln et al. 2007), suggesting that the *M. tuberculosis* relies on de novo synthesis as the only source of biotin. Although feeding studies also indicate that TB can take up biotin from the media, it requires higher concentrations (micromolar) than *E. coli* (picomolar).

Biotin is synthesized in a multistep pathway divided into two stages, as shown in figure 1. The first is non-conserved, whereas the second stage is conserved in biotin-producing organisms. In *E.coli*, the first stage reactions are catalyzed by the enzymes BioC and BioH, leading to the generation of pimeloyl CoA precursor. *M. tuberculosis* is predicted to use the same enzymes due to the presence of BioC and BioH gene homologs in the *M. tuberculosis* genome (Salaemae et al., 2011). The synthesis of biotin in the conserved stage begins with alanine and pimeloyl ACP or pimeloyl CoA as precursors. The enzyme 7-keto-8-aminopelargonic acid synthase (BioF) catalyzes the decarboxylation of L-alanine and the condensation of the resulting carbanion with the thioester carbonyl of pimeloyl CoA, resulting in the formation of the ketone of 7-keto-8-aminopelargonic acid (KAPA). 7,8-Diaminopelargonic acid synthase (BioA) converts KAPA to 7,8-diaminopelargonic acid (DAPA) through a transamination reaction using S-adenosyl-L-methionine (SAM) as the amine donor. In the penultimate step, CO_2 spontaneously reacts with DAPA to form a carbamic acid, which undergoes an ATP-dependent ring closure to form the ureido ring of dethiobiotin (DTB) catalyzed by dethiobiotin synthase (BioD) (Huang et al., 1995). Finally, biotin synthase (BioB), a radical SAM enzyme, inserts a sulfur atom at the methylene and methyl carbons at positions C6 and C9 of DTB to form biotin (Cramer et al., 2018).

Various mutagenesis studies have confirmed the importance of the biotin biosynthetic pathway to the growth and survival of *M. tuberculosis*. Studies have shown that the disruption of BioA impaired the survival of *Mycobacterium smegmatis* during the stationary phase on carbon-depleted media (Keer et al., 2000; Sassetti et al., 2001). Disruption of BioF and BioB hinders bacterial growth during and post-infection of murine macrophages (Rengarajan et al. 2005). Also, a small molecule inhibitor, CID 1245700, has been shown to inhibit BioA and is effective at killing TB in lab cultures (Casalena et al., 2010).

Biotin Synthase

Biotin synthase (BioB) catalyzes the final step in biotin biosynthesis by converting dethiobiotin to biotin. BioB is an *S*-adenosyl-L-methionine (SAM) dependent enzyme that employs a radical mechanism. BioB is a homodimer with the active site of each monomer containing a $[4Fe\text{-}4S]^{2+}$cluster, SAM, and a $[2Fe\text{-}2S]^{2+}$cluster, as shown in figure 2. The $[4Fe\text{-}4S]^{2+}$cluster is directly coordinated with SAM and three cysteine residues. The $[2Fe\text{-}2S]^{2+}$ cluster is ligated by three cysteines and an arginine residue (Berkovitch et al., 2004). SAM radical enzymes such as BioB accept one electron from an external electron donor as the first step in a radical generation. In *E. coli*, NADPH, flavodoxin reductase, and flavodoxin 1 have been established as the essential electron transfer system(Birch et al., 1995; Ifuku et al., 1994). Even though ferredoxin and flavodoxin 2 are present in *E. coli*, they cannot substitute for flavodoxin 1 in the electron transfer system (Wan et al & Jarrett, 2002).

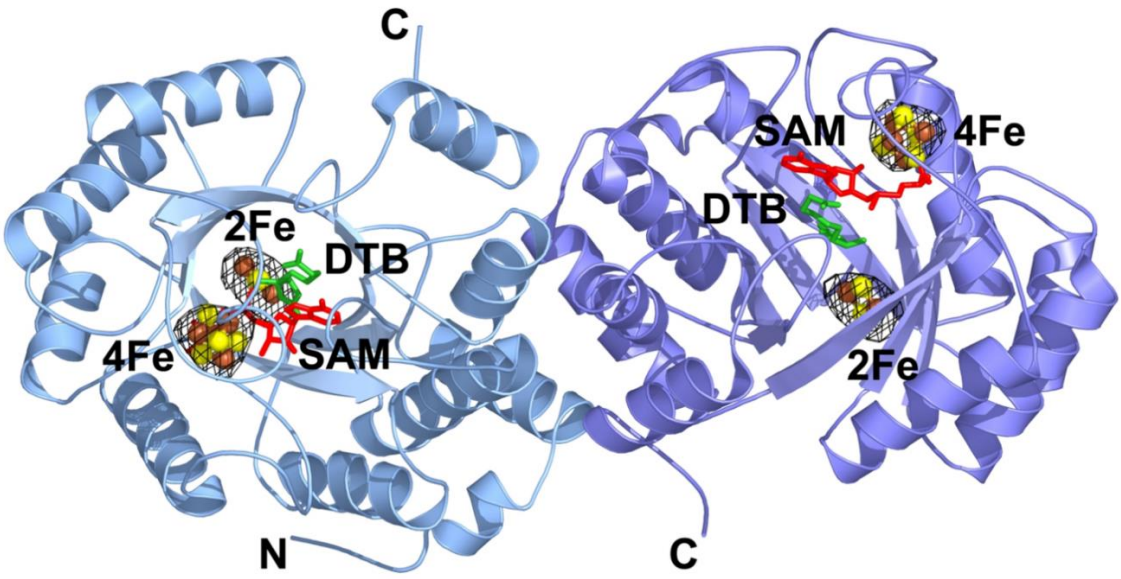

Figure 2. Crystal structure of the *E. coli* biotin synthase homodimer in complex with [2Fe-2S] and [4Fe-4S] clusters, dethiobiotin (green), and S-adenosylmethionine (red) (Berkovitch et al., 2004).

The BioB mechanism begins with the $[4Fe–4S]^{2+}$ cluster accepting one electron from a reduced flavodoxin and transferring the electron to SAM (Guianvarc'h et al., 1997). The $4Fe\text{-}4S]^{2+}$cluster gets reduced, and SAM is spontaneously cleaved to generate a 5'-deoxyadenosyl radical and methionine. The generated radical abstracts a hydrogen atom from dethiobiotin, forming a dethiobiotinyl C9 carbon radical, which immediately is quenched by bonding to a sulfur atom on the $[2Fe\text{-}2S]^{2+}$ cluster (Ugulava et al., 2000) and reducing one of the iron atoms from Fe(III) to Fe(II). Reductive cleavage of a second SAM molecule generates another 5'-deoxyadenosyl radical, which abstracts a hydrogen atom from C6 of dethiobiotin, forming a carbon radical that attacks the same sulfur atom on the $[2Fe–2S]^{2+}$ cluster, forming the thiophane ring. The $[2Fe–2S]^{2+}$ cluster is destroyed after one enzyme turnover (Ugulava , Sacanell, et al., 2001).

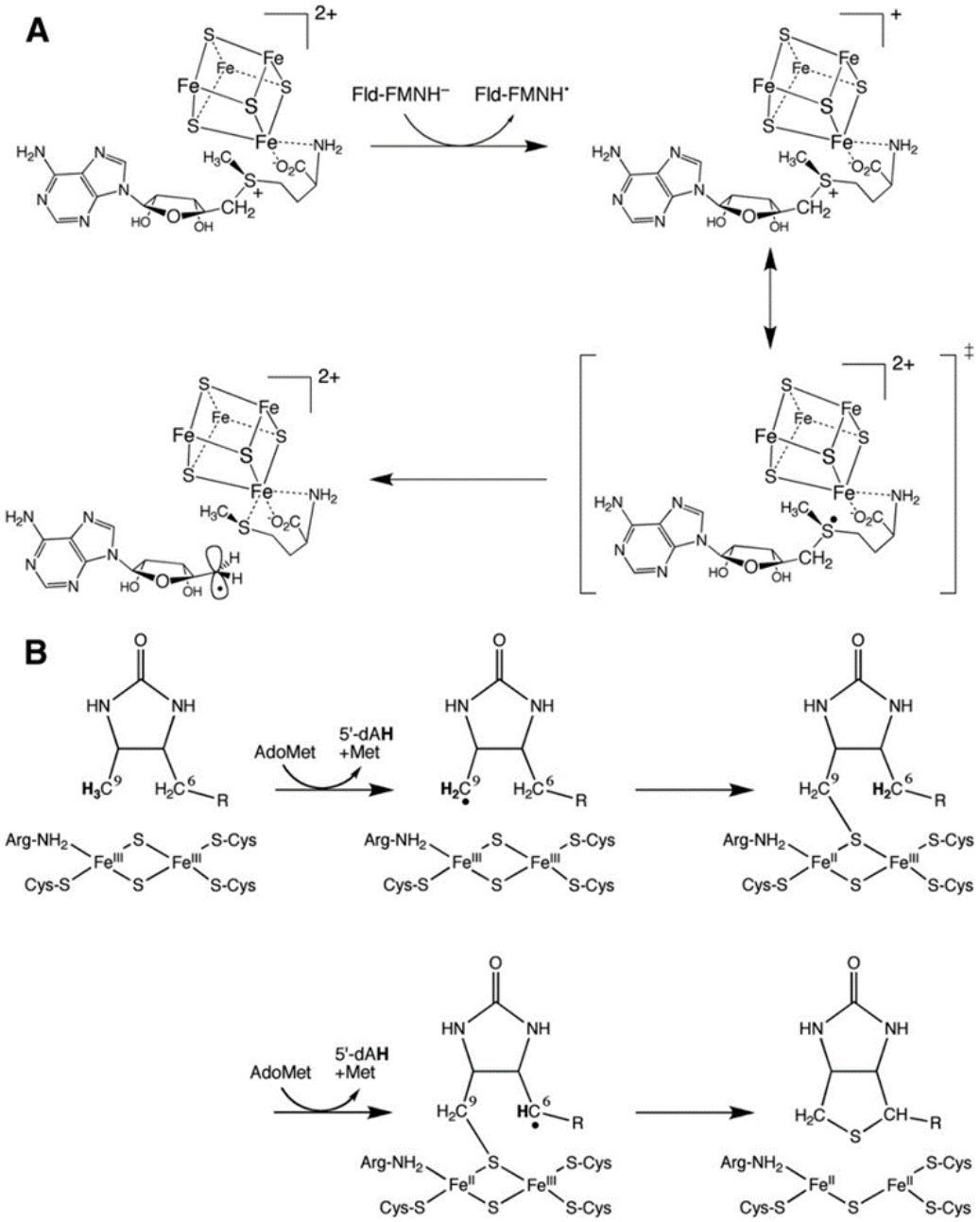

Figure 3. Proposed biotin synthase mechanism. **(A)** Electron transfer from reduced flavodoxin via the [4Fe–4S]2+ onto SAM. **(B)** Sulfur insertion into dethiobiotin to form biotin (Fugate & Jarrett al, 2012).

Two assembly systems, ISC (iron-sulfur cluster) and SUF (sulfur mobilization), are responsible for the biogenesis of the iron-sulfur cluster in prokaryotes. The operon for the ISC encodes the proteins IscS, IscU, IscA, HscA, HscB, and Fdx. SUF operon contains the proteins SufA, SufB, SufC, SufD, SufS, and SufE . SufS and SufA are homologs of IscS and IscA, respectively. For ISC, iron-sulfur cluster assembly starts with the production of S-sulfide sulfur from cysteine by the cysteine desulfurase IscS. The sulfur moiety is to IscU. Ferrous iron binds to IscU, forming a [2Fe–2S] cluster, which can generate a [4Fe–4S] cluster. HscA, HscB are chaperones that interact with IscU. Fdx IS a [2Fe– 2S] ferredoxin involved in electron transfer during the iron-sulfur cluster assembly (Cammack, 2013).

Biotin Synthase Gene Cluster

In *M. tuberculosis*, two genes, Rv1590 and Rv1591, are appended to the biotin synthase gene, as illustrated in figure 4 (Kapopoulou et al., 2011). These two genes are conserved in all actinobacteria.

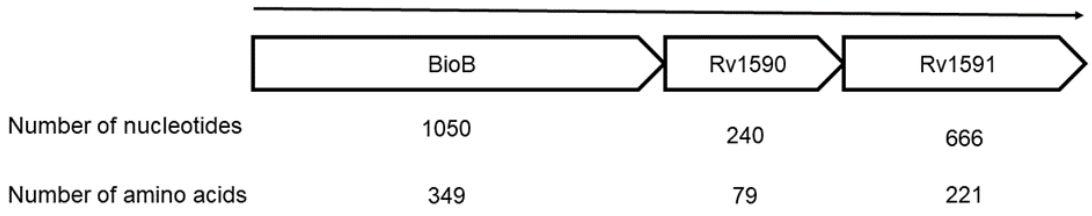

Figure 4. Organization of the BioB, Rv1590, and Rv1591 genes and their gene products in *M. tuberculosis*.

The conservation of these genes in actinobacteria suggests that they may have essential functions. However, Himar1 transposon studies have shown that both genes are non-essential for *in vitro* growth of the H37Rv strain of *M. tuberculosis* (DeJesus et al., 2017; Sassetti et al., 2003). However, these studies were performed using the transposon site hybridization method, a screening tool that does not consider the growth requirement for individual genes. One study on C57BL/6J mouse spleen medium shows that Rv1590 is required for growth in H37Rv (Sassetti & Rubin, 2003). More experiments with defined growth conditions are necessary to elucidate the importance of these genes. Rv1591 has been identified in the membrane fraction of *M. tuberculosis H37Rv* using 1D-SDS-PAGE and ULC-MS/MS and is predicted to be a membrane protein(Gu et al., 2003).

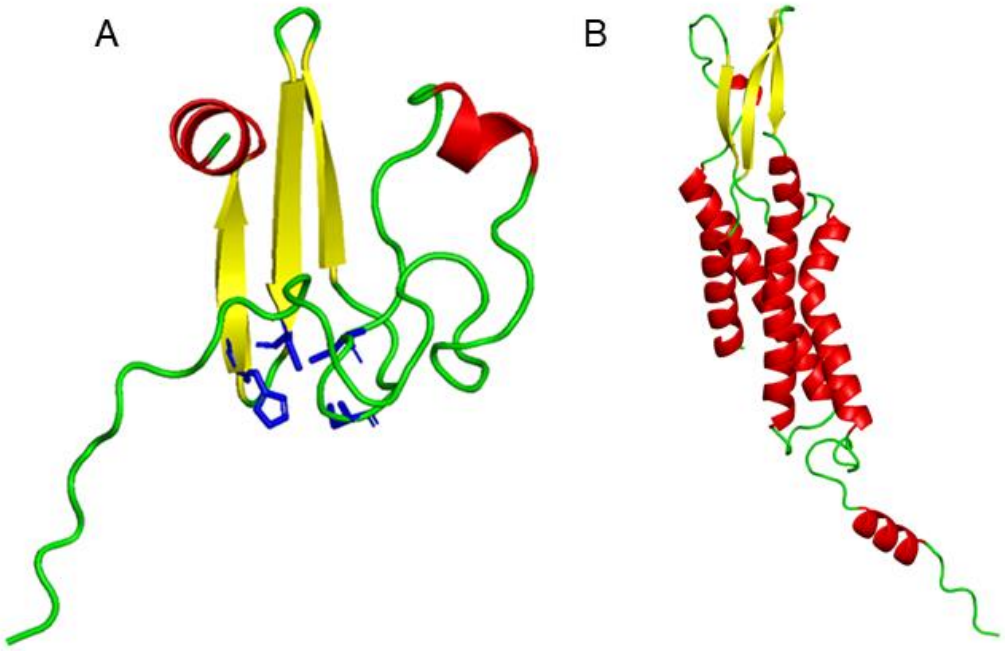

Figure 5. AlphaFold 2 predicted secondary structures illustrated using PyMol: **(A)** Rv1590 and **(B)** Rv1591. Beta sheets (yellow), alpha helices (red), random coils (green), and metal ligands (blue).

Structures of both proteins shown in figure 5 have been predicted using AlphaFold 2 (Jumper et al., 2021). Rv1590 is predicted to be a rubredoxin because it possesses the features of rubredoxins: three antiparallel b-strands and two loops containing a metal coordination site comprised of three cysteines and one histidine. Rv1591 comprises three alpha helices (possibly membrane-spanning) and three antiparallel beta strands. Further structural studies are required to elucidate the structures of both proteins.

The biological functions of both proteins have not been established, and we hypothesize two possible functions for Rv1590: an electron donor in biotin synthase reaction or part of the iron-sulfur cluster repair system. In *E. coli*, biotin synthase catalysis requires flavodoxin for electron transfer (Ifuku et al., 1994). *In vitro* studies have shown that *E. coli* flavodoxin does not support the activity of *M. tuberculosis* biotin synthase (J. Cramer, 2018). We hypothesize that Rv1590 may play the role of an external electron donor in *M. tuberculosis*. *E.coli* biotin synthase has a turnover rate of less than one (Tse Sum Bui et al., 2004) due to the destruction of the $[2Fe\text{-}2S]^{2+}$ cluster, which is the supplier of the sulfur for the biotin thiophane ring (Farrar et al., 2010). Further studies suggested that the IscU and HscA proteins of the ISC iron-sulfur cluster assembly system were essential to regenerate active BioB in E. coli (Reyda et al, Fugate and Jarrett, 2009. Therefore, reconstitution of the $[2Fe\text{-}2S]^{2+}$ cluster is necessary for biotin synthase to achieve multiple turnovers. *E. coli* biotin synthase is capable of up to 20 turnovers *in vivo* due to the presence of the ISC and Suf systems (Choi-Rhee et al& Cronan, 2005) that can perform Fe-S cluster assembly and repair. In *M. tuberculosis*, the Suf system is the Fe-S cluster assembly pathway (Huet et al., 2005). An alternative hypothesis is that Rv1590 may be a specific mediator of this cluster reconstitution for BioB.

Rubredoxin

Rubredoxins are the simplest non-heme iron proteins, typically containing a single iron ion tetrahedrally coordinated to four cysteine residues in their active sites (Sieker et al., 1994). Rubredoxins are considered iron-sulfur proteins because of the cysteinyl sulfur ligands, even though they do not contain acid-labile sulfide like other iron-sulfur proteins. Lovenberg and Sobel isolated the first rubredoxin in 1965 from the anaerobic bacterium *Clostridium pasteurianum*. After 1965, rubredoxins have been isolated and characterized from many different species, such as the eukaryotic rubredoxin from the unicellular algae *Guillardia theta* (Wastl et al., 2000) and archeal rubredoxin from *Pyrococcus furiosus* (Jenney & Adams, 2001). Most well-characterized rubredoxins contain a single ferric or ferrous iron ion in their active sites. However, rubredoxin from *Pseudomonas oleovorans* has been found to have two similar domains containing two-iron centers with less stability than the one-iron rubredoxin (Perry et al., 2004)

The structures of various rubredoxins have been solved by x-ray crystallography (Adman et al., 1991; Dauter et al., 1996) and in the solution state by NMR spectroscopy (Perry et al., 2004). Figure 6 shows the structure of rubredoxin from *Clostridium pasteurianum*. Rubredoxins are composed of short, three antiparallel b-sheets, two loops containing the four cysteine residues that tetrahedrally coordinate the metal atom, and a hydrophobic core made up of conserved aromatic residues that stabilize the protein (J. Meyer & Mouliset al, 2006). The structure is also composed of charged residues regularly distributed over the molecule's surface except for the metal binding site (J. Meyer & Moulis, 2006).

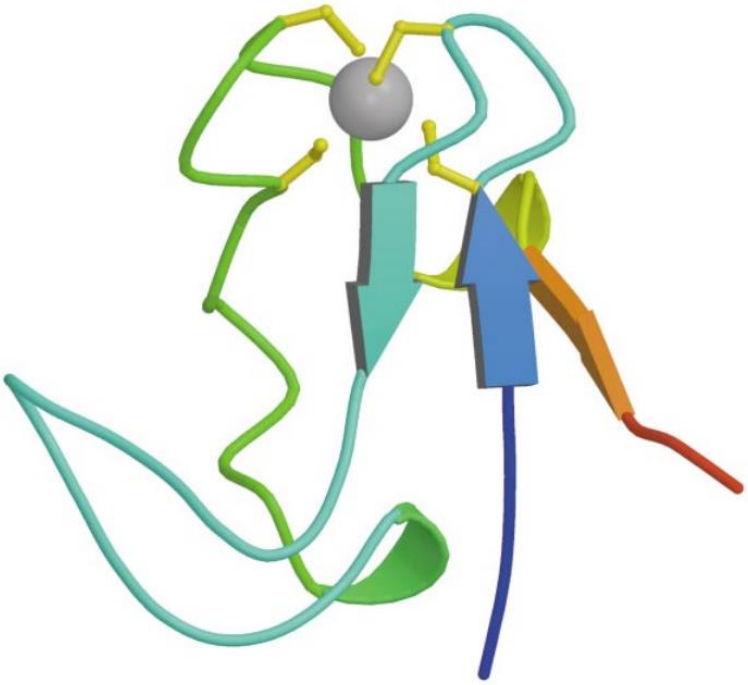

Figure 6. 3D ribbon diagram of rubredoxin from *Clostridium pasteurianum* showing the iron atom (grey sphere) ligated by cysteine residues (yellow) (J. Meyer & Moulis, 2006).

The primary biological role of rubredoxin is not well understood. It is widely accepted that they participate in electron transfer processes due to the presence of the redox-active iron center. Some studied roles include carbon fixation (Ragsdale et al., 1983), removal of reactive oxygen species (Kurtz, 2004), fatty acid metabolism (Yoon et al., 1999), and hydrogen oxidation in *Azotobacter vinelandii* (Chen et al. & Mortenson, 1992; Gomes et al., 1997). Rubredoxin in *Pseudomonas oleovorans* is proposed to serve as an electron carrier from a soluble flavoprotein (reductase) to a membrane-bound alkane hydroxylase in the alkane hydroxylation system (Haspel et al., 1995; Peterson et al.& Coon, 1968).

The redox potential of several rubredoxins has been investigated through different methods. The two redox states are Fe (II) and Fe (III) for the reduced and oxidized states, respectively (Eaton & Lovenberg, 1973). Variations in the redox potential have been reported in different proteins despite sharing a common metal coordination geometry (Gilep et al., 2022a). Rubredoxins have redox potentials ranging from –100 to +100 mV (vs. SHE) (−300 to −100 mV vs. Ag/AgCl) (Gilep et al., 2022a). The variation in redox potential is thought to be determined by several factors, including the active site structure, hydrogen bonding pattern around the active site, and the electrostatic environment (Swartz & Ichiye, 1997).

Two rubredoxin genes, Rv3251c and Rv3250c, have been identified in *M. tuberculosis*. Rv3251c encodes a 55 amino acid residue protein (rubredoxin A), and Rv3250c encode a 60 amino acid residue protein (rubredoxin B). The gene for rubredoxin B is repressed *in vitro* under mildly acidic and hypoxic conditions that mimic the state of a dormant bacterium (Kim et al., 2008). The solution structure for rubredoxin B has been solved after substituting iron with zinc (Buchko et al., 2011). Rubredoxin B has been characterized with a redox potential of −264 mV (vs. Ag/AgCl) (Gilep et al., 2022a) and possesses the ability to transfer an electron from different NAD(P)H-dependent reductases to cytochrome P450 enzymes, CYPs (Sushko et al., 2021).

Scope of My Research

Due to the conservation of the Rv1590 and Rv1591 genes in mycobacteria, it is essential to characterize them and determine their importance in mycobacteria, specifically their potential role in the reaction catalyzed by biotin synthase. This project is

the first attempt to clone the Rv1590 gene, express the encoded protein in an *E. coli* expression strain, purify Rv1590 both as a SUMO fusion protein and the native protein, and to characterize the properties of the resulting metalloprotein.

CHAPTER 2: METHODOLOGY

Bioinformatics

Bioinformatics tools were used to study the structure and function of Rv1590 due to the lack of structural data from X-ray crystallography or NMR. The protein sequence was obtained from UniProt using the gene identifier Rv1590 and used for Basic Local Alignment Search Tool (BLAST) to obtain homologous protein sequences to Rv1590. Blast search was done using Blastp with an E-value of 0.001 and a search limit of 100 hits. The 100 sequences obtained from the BLAST search were aligned to identify conserved amino acid residues.

Amino acid sequences for rubredoxins with solved crystal structures were obtained from GenBank. ClustalW alignment (Sievers et al., 2011) was done for the rubredoxins and Rv1590 to identify sequence similarities. ClustalW uses the BLOSUM weight matrix to determine the similarity of divergent protein sequences. ClustalW first constructs a dendrogram, like a phylogenetic tree, by grouping the sequences based on similarity in a pairwise alignment. A multiple-sequence alignment is performed using the dendrogram as a guide. For this project, a gap penalty of 3 was used with a percent identity scoring method for pairwise alignment. For multiple alignments, a gap open penalty and gap extension penalty of 10 and 0.05 were used, respectively. The predicted three-dimensional structure of Rv1590 was downloaded directly from the AlphaFold protein structure database (Jumper et al., 2021) as a PDB file and visualized in PyMOL.

Molecular Cloning

Molecular cloning techniques were used to insert the Rv1590 gene into the chosen bacterial plasmid and replicate the recombinant DNA in *Escherichia coli (E. coli).* A polymerase chain reaction (PCR) was done to amplify the gene and the plasmid DNA, followed by restriction enzyme digestion and ligation. The ligation product (Recombinant DNA) was transformed into *E. coli* competent cells. The recombinant DNA was replicated in the host and purified.

Choice of Plasmid

A plasmid is a small circular DNA molecule found in bacteria and other microscopic organisms that can replicate independently from the host's chromosomal DNA. A gene of interest can be inserted into the plasmid using molecular cloning to create a recombinant plasmid. When the plasmid is inserted into a host organism, it can replicate within the host, making copies of the inserted gene. Plasmids also contain a promoter region that drives the transcription of the cloned gene for recombinant protein expression and purification. A vector is an artificially made plasmid for cloning, amplifying, and expressing a target gene (Russell DW, 2001). The pETHSUL vector (Figure 6) was used for cloning and protein expression in the project. pETHSUL plasmid was designed by incorporating a small ubiquitin-like modifier (SUMO) sequence from the *Saccharomyces cerevisiae* strain RSY335 into pET21 plasmid (Weeks et al., 2007). SUMO increases the recombinant protein's solubility in *E. coli* (Marblestone, 2006). In the pETHSUL plasmid, the SUMO is affinity tagged with His_6 to allow for purification using immobilized metal

affinity chromatography (IMAC). The His_6-SUMO tag can be cleaved using a recombinant SUMO protease (Malakhov et al., 2004) to yield the mature protein of interest. The plasmid also has an ampicillin resistance gene for the selective growth of the bacteria.

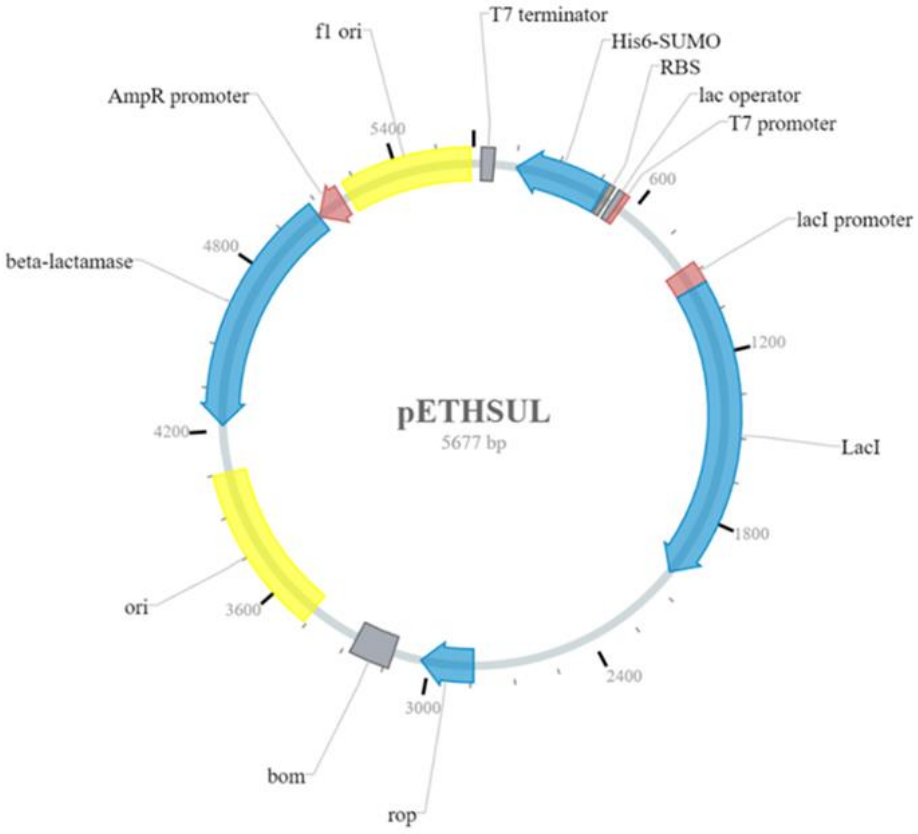

Figure 6. pETHSUL vector map (https://novoprolabs.com/vector/Vgyytemq)

Primer Design

Before cloning, multiple copies of the plasmid DNA and the gene of interest must be obtained. DNA Amplification is made possible through a polymerase chain reaction

(PCR). The first step in amplifying DNA is to design primers, short single-stranded DNA sequences complementary to the ends of the DNA to be amplified. Prof. Jarrett designed the primers for this project, shown in table 1. The primers were designed using parts of the pETHSUL plasmid (pETHSUL primers) and the *M. Tuberculosis* (Rv1590 primer) genomic DNA sequences. HindIII restriction site was added to the pETHSUL forward primer and Rv1590 reverse primer. BamHI restriction site was added to the pETHSUL reverse primer and Rv1590 forward primer. The restriction sites were used for the subsequent ligation of the gene into the plasmid. The first amino acid, methionine, was excluded from the Rv1590 forward primer.

Table 1. pETHSUL and Rv1590 primers. The letters F and R in the primer names indicate forward and reverse, respectively. Restriction sites in the sequences are in bold.

Primer name	**Sequence 5'-3'**	**Melting Temp (°C)**
pETHSUL-HindIII-F	CGAG**AAGCTT**CTGCTAACAAAGCCC	60.0
pETHSUL-BamHI-R	TTTA**GGATCC**ACCAATCTGTTCGCGGTG	62.2
Rv1590-BamHI-F	ATAT**GGATCC**GTGGAAATCGTGGCTGGAAAA CAAC	64.2
Rv1590-HindIII-R	ATAT**AAGCTT**CATCGCTGTGTCGCCAAGTC	61.8

Polymerase Chain Reaction

A polymerase chain reaction was used to make copies of the pETHSUL vector and Rv1590 gene. The PCR reaction mixtures were set up as shown in table 2 using the previously designed primers. The *M. tuberculosis* genomic DNA, and pETHSUL plasmid DNA were used as templates. The thermocycler reaction conditions are shown in table 3.

Table 2: Set-up mixture for PCR reaction

Reagents	**Volume (uL)**	**Final concentration**
PrimeSTAR Premix (2X)	25	1X
Forward Primer	1.5	0.3ng
Reverse Primer	1.5	0.3ng
Template DNA	1	10ng
Nuclease free water	21	N/A
Total volume	50	

Table 3. Thermocycler program conditions

Step	**Temperature (°C)**	**Time (sec)**	**Number of cycles**
Initial denaturation	95	160	1
Denaturation	95	10	30
Annealing	55	30	30
Extension	72	30	30
Hold	0	Infinite	

Agarose Gel Electrophoresis

Agarose gel electrophoresis was used to separate and identify the DNA from the PCR reactions. 50x TAE buffer was made by dissolving 242 g Tris base, 18.6 g EDTA, and 57.1 mL glacial acetic acid in water to a final volume of one liter. A 1% (w/v) agarose gel was prepared by dissolving 0.5 g of agarose in 50 mL of 1x TAE (Tris-acetate-EDTA) buffer. The agarose-TAE mixture was heated in the microwave until all the solids were dissolved. The mixture was then cooled to approximately 50 °C, poured into a gel cassette with combs inserted, and let sit until solidified (about 30 minutes). 2 uL of the PCR products were mixed with 1 uL of 6x GelRed Prestain loading dye and 15 uL of deionized water to a total volume of 20 uL. The samples (20 uL) were loaded into each well in the gel. The GeneRuler DNA ladder (5uL) was loaded in a separate well alongside the samples. The agarose gel was run at a constant voltage of 100V for 1.5 hours and visualized on a dual-intensity UV transilluminator.

PCR Clean Up

Before downstream use, the PCR products were purified using a Promega PCR cleaned-up kit to remove primers, nucleotides, enzymes, and buffer components. After clean-up, a NanoDrop spectrophotometer (Thermo Fisher Scientific) was used to quantify the DNA.

Table 4. Restriction enzyme digestion mixture

	Insert	**pETHSUL vector**
Buffer	5	5
Insert	12	-
pETHSUL	-	12
BamHI	1	1
HindIII	1	1
DpnI	1	1
TSAP	-	1
Sterile water		
Total	50	50

Restriction Enzyme Digestion

The amplified pETHSUL plasmid and Rv1590 gene were incubated with the BamHI and HindIII restriction enzymes to cleave the DNAs at the specific sites added during primer design. Restriction enzyme digestion creates sticky ends which are ligated to clone the gene into the plasmid. Restriction enzyme cleavage was set up as shown in table 4, and the reaction was incubated at 37 °C for 4 hours. DpnI was added to digest the excess template DNA by cleaving the *E. coli* methylated DNA. TSAP, thermostable alkaline phosphatase, was added to catalyze the dephosphorylation of the 5' and 3' ends of the sticky DNA phospho-ends generated after digestion. Dephosphorylation prevents the relegation of the linearized plasmid after digestion. After digestion, the samples were

purified using the Promega PCR cleaned-up kit, and concentrations were determined using the NanoDrop spectrophotometers (Thermo Fisher Scientific).

DNA Ligation

Rv1590 gene was ligated into the vector using Promega T4 DNA ligase in a 1:3 molar ratio of vector: insert using 50 ng of the vector. The following calculation was used to convert molar ratios to mass ratios using a 50 ng plasmid vector. The reaction was set up in a sterile microcentrifuge tube, as shown in table 5, and incubated at room temperature overnight.

Table 5. Ligation reaction mixture (https://www.neb.com/protocols/0001/01/01/dna-ligation-with-t4-dna-ligase-m0202)

	Volume (µl)
Vector DNA	2.5
Insert DNA	1
10X Ligase Buffer	1
T4 DNA Ligase	1
Milli Q water	4.5
Total	10

Making DH5α Competent Cells

E. coli strain DH5α cells were made competent to take in exogenous DNA. 5 mL Lennox lysogeny broth (LB) was inoculated with a single colony of *E. coli* DH5α cells from an LB plate and incubated for 12 hours at 37 °C with shaking at 225 rpm. 50 mL of LB was inoculated with 100 uL of the overnight culture, and cells were grown at 37 °C until OD_{600} was approximately 0.2. The cells were chilled on ice for 10 minutes and centrifuged at 5000 rpm for 8 minutes. The cell pellet was resuspended in 5 mL of ice-cold 0.1 M $CaCl_2$ and centrifuged at 4000 rpm for 5 minutes. The cell pellet was resuspended in 1 mL of 0.1 M $CaCl_2$ in a sterile falcon tube and incubated for more than one hour before use, and extra cells were stored at 4 °C. For freezing, the cell pellet was resuspended in 1 mL of 0.05M $CaCl_2$, mixed with an equal volume of 40% sterile glycerol, divided into ~0.5 mL aliquots into 1.5 mL Eppendorf tubes, flash frozen in dry ice-ethanol bath, and stored in a -80 °C freezer.

Transformation of *E. coli* DH5α Cells

The recombinant plasmid created by ligating the Rv1590 gene into the pETHSUL vector was inserted into the host, *E. coli*, using the heat shock method. 50 uL of the *E. coli* DH5α competent cells were aliquoted into sterile 1.5 mL microcentrifuge tubes, and 2 uL (10ng) of DNA was added to the cells and gently mixed. After 30 minutes of incubation on ice, the cells were subjected to heat shock for 60 seconds in a 42 °C water bath and immediately placed on ice for 5 minutes. To each tube, 950 uL of sterile pre-warmed LB media was added, and cells were incubated at 37 °C for 1 hour with shaking

at 225 rpm. 200 uL from each transformation was spread on pre-warmed ampicillin selective LB agar plates and incubated overnight at 37 °C.

Recombinant DNA Purification

Recombinant DNA, made of the pETHSUL plasmid ligated to the Rv1590 gene, was purified from the transformed *E. coli* DH5α cells. 10 ml of LB media containing 100 mg/ml of ampicillin was inoculated with a single colony from an LB agar plate of the previously transformed cells. The cells were grown overnight at 37 °C with shaking at 225 rpm. The Recombinant DNA was purified from the overnight culture using a Promega miniprep DNA purification system. PCR amplification was done using the purified recombinant DNA as the template and the Rv1590 primers to confirm the ligation of the gene into the plasmid. Sequencing was done at the Advanced Studies in Genomics, Proteomics, and Bioinformatics (ASGPB) facility at the University of Hawaii at Manoa. Samples were prepared by PCR reactions using the T7 promoter and T7 terminator as primers.

Protein Expression and Purification

Small-Scale Expression

The purified recombinant DNA was transformed into *E. coli* BL21(star) competent cells using the previously described heat shock method. Small-scale expression of

Rv1590 was done to test for protein expression conditions. A single colony of *E. coli* BL21(star) from the LB agar plate was used to inoculate 10 mL LB with 100 ug/mL of ampicillin and cells grown overnight at 37 °C. 50 mL of LB was inoculated with 5 mL of the overnight culture and incubated at 37 °C with shaking at 225 rpm until OD_{600} was 0.4-0.6. Protein expression was induced by adding isopropyl β-D-1-thiogalactopyranoside (IPTG) at a final concentration of 0.5 mM, and cells were grown for 4 hours at 37 °C. The cells were harvested by centrifugation at 6000 rpm for 10 minutes. The supernatant was discarded, and the cell pellet was resuspended in 5 mL of 50mM Tris buffer pH 8.0. The cells were sonicated using a Fisher model 505 sonic dismembrator at 80% power with 4 cycles of 30 s on and 120 s. The sonicate was centrifuged at 15000 rpm for 15 min at 4 °C. 10 uL of the supernatant was taken for SDS-PAGE analysis. The pETHSUL plasmid without the Rv1590 gene inserted was expressed under the same conditions as a negative control.

SDS-PAGE Gel Electrophoresis

SDS-PAGE gel electrophoresis was done using a 12% sodium dodecyl sulfate-polyacrylamide gel to separate and identify the components of the protein mixture based on their size. The resolving and stacking layers were made using lower and upper tris buffer, respectively. Lower tris buffer was made by dissolving 90.89 g Tris base in 400 mL of distilled water, and the pH was adjusted to 8.8 with 6N HCl. The mixture was brought up to a final volume of 500 mL, and filter sterilized. Upper tris buffer was made by dissolving 6.06 g Tris base in 80 mL of distilled water, and the pH was adjusted to 6.8 with 6N HCl. The mixture was brought up to a final volume of 100 mL, and filter sterilized.

The 12% SDS-PAGE gel was made using a 4% stacking layer and a 12% resolving layer. The resolving layer was made by mixing 6.32 mL of water, 3.75 mL of lower tris buffer, 4.69 mL of 40% Acrylamide solution, 150 uL of 10% SDS, 75 uL of 10% ammonium persulfate solution, and 15 uL of tetramethylethylenediamine (TEMED). The mixture was poured into the cassette, and deionized water was added to the polymerizing layer to ensure a level surface. After polymerization (about 1 hour), the 4% stacking layer was made by mixing 4.74 mL of water, 1.89 mL of upper tris buffer, 0.75 mL of 40% acrylamide solution, 75 uL of 10% SDS, 37.5 uL of 10% ammonium persulfate and 7.5 uL TEMED. The water on top of the polymerized resolving gel was removed, the gel combs were inserted into the cassette, and the stacking layer mixture was poured. The gel was left to stand for 1 hour to solidify.

The 5 x sample buffer was made by mixing 9.38 mL of lower tris buffer, 1.5 g of SDS, 18.8 mL of glycerol, and 7.5 mg of bromophenol blue in 28.5 ml of water. The buffer was aliquoted into 0.95 mL per eppendorf tube and frozen at -20 °C. When needed, one tube was thawed, and 50 uL of β-mercaptoethanol (BME) was added and kept at room temperature. The 5X running buffer was made by dissolving 15.2 g Tris HCl, 72.1 g glycine, and 10.0 g SDS in 1 liter of deionized water and stored at room temperature.

When loading purified protein samples, 5 uL of the 5 x sample buffer was added to the samples and heated at 95 °C for 5 minutes before loading the gel. 5 uL of PAGEmark Tricolor PLUS protein Ladder (G Biosciences) was used as a standard in all SDS-PAGE gels. The Bio-Rad PowerPAC power supply and Mini-PROTEAN Tetra Cell were utilized to run all the SDS-PAGE electrophoresis. The power supply was set to a constant voltage

of 100V and run for 60 minutes. The gels were rinsed with deionized water and stained with a Coomassie stain for 1 hour. The gel was destained until bands were visible.

Large-Scale Expression

After successful small-scale expression, large-scale expression was carried out for protein purification. A single colony of *E. coli* BL21(star) transformed with the recombinant DNA was used to inoculate 10 mL LB media supplemented with 100 ug/ml of ampicillin. The cells were grown overnight at 37 °C while shaking at 230 rpm. One liter of minimal media in a 2.8 L Erlenmeyer flask was inoculated with 5 mL of the overnight culture. The media was supplemented with 100 ug/mL of ampicillin and 50 ug/mL of ferrous ammonium sulfate. The cells were grown at 37 °C while shaking at 230 rpm until an OD_{600} of 0.6-0.8 was reached (approximately 4 hours). The temperature was lowered to 25 °C for 30 minutes before IPTG was added to a final concentration of 0.5 mM. The cells were grown for 16 hours while shaking at 230 rpm and harvested by centrifugation at 5000 rpm for 10 minutes. The supernatant was discarded, and the cell pellet was weighed and frozen at -80°C.

Protein Purification

The frozen cell pellet was thawed and resuspended in lysis buffer (50 mM Tris, 500 mM NaCl, pH 8.0), 3 mL buffer per gram of cell. Cells were transferred to a 150 mL glass beaker, cooled on ice, and lysed by sonication using a Fisher model 505 sonic dismembrator with a 0.5-inch diameter probe at 80% power with 4 cycles of 30s on/120s off. The cell lysate was transferred to centrifuge bottles, and the insoluble debris was

pelleted by centrifugation at 40,000 rpm for 60 min at 4°C in an L-80 ultracentrifuge (Beckman). A Nickel NTA Superflow column (Qiagen) was washed with 0.1 M tetrasodium EDTA, recharged with 0.1 M $NiCl_2$, and equilibrated with equilibration buffer (50 mM Tris, 500 mM NaCl, 5 mM imidazole, pH 8.0). The clarified cell lysate was loaded onto the Ni-NTA column at a flow rate of 1 mL/min. The column was washed with the equilibration buffer until the UV detector (280 nm) showed a flat baseline (approximately 200 mL of buffer). The bound protein was eluted with elution buffer (50 mM Tris, 500 mM NaCl, 200 mM imidazole, pH 8.0) until the UV detector (280 nm) established a flat baseline (about 60 mL of buffer for a 4 L culture). The protein was concentrated to about 15 mL by centrifugation in Amicon Ultra-15 10 kDa centrifugal filters. BioGel G25 column was equilibrated with the storage buffer (50 mM Tris, 500 mM NaCl, pH 8.0), and the concentrated protein was loaded onto the column at a flow rate of 3 mL/min. The protein was collected in the flow through, and the column was washed with the storage buffer until all the protein was eluted. The desalted protein was concentrated to <10mL.

The purified fusion protein was cleaved using SUMO protease to remove the His_6-SUMO tag. The protease was added at a ratio of 1 mg of protein to 1 ug of protease, and the cleavage reaction was done at room temperature for 12 hours. The Ni-NTA column was equilibrated with the storage buffer, and the cleavage mixture was loaded at a flow rate of 1 mL/min. The flow-through (pure Rv1590) was collected while the His_6-SUMO and protease remained bound to the column and were eluted using the elution buffer. The pure Rv1590 was concentrated in 3 kD centrifuge filters, aliquoted, and frozen in a -80 °C freezer when not used immediately.

Protein Characterization

UV-Visible Spectroscopy

The absorption spectra in the near UV visible wavelength (250–800 nm) were collected on a Varian 50 Bio UV-Visible Spectrophotometer in a 1 mL quartz cuvette of 1 cm path length at 25 ^{o}C.

Protein Quantitation

The protein concentration was calculated using absorbance at 280 nm of the denatured protein. Denaturation was done by mixing 100 uL of the protein with 900 uL of 6 M guanidine hydrochloride. A blank was prepared by mixing a storage buffer. Absorbance at 280 nm was obtained using a 1 mL quartz cuvette of 1 cm path length on the Varian 50 Bio UV-Visible Spectrophotometer. The protein extinction coefficient (15470 $M^{-1}cm^{-1}$) was computed using the protein analysis tool ProtParam on the ExPASy server, and the protein concentration was calculated using Beer-Lambert's law.

Molecular Weight Determination

The molecular weight of the pure protein was determined using mass spectroscopy in the chemistry department at the University of Hawaii. The protein sample was prepared at a final concentration of 1 mg/mL in 50 mM Tris-HCl, 500 mM NaCl pH 8.0 buffer. Mass spectra were acquired via electrospray ionization in the positive mode using an Agilent 6545 Q-TOF LC/MS equipped with Agilent 1290 Infinity series binary HPLC. Liquid

chromatography was done using a reversed-phase gradient with a ZORBAX RRHD Eclipse Plus C18, 95Å, 2.1 x 50 mm, 1.8 µm column at a flow rate of 0.5 mL/min and UV detection at 280 nm. The solvents used were water (solvent A) and acetonitrile (solvent B), both in 0.1% formic acid. 10 % solvent B was run for 0.5 minutes, followed by a gradient from 10% to 100% in 3.5 minutes. Solvent B was held constant at 100% for 4 minutes before the gradient was run back to 10 % in 1 minute.

Sodium Dithionite Reduction

Sodium dithionite reduction was done under anaerobic conditions in a quartz cuvette.100 µM protein sample was sufficient to properly visualize the 409 nm peak of Rv1590 used to monitor the protein reduction. The protein sample was purged with nitrogen for 10 minutes in a sealed 1 mL cuvette to remove the dissolved oxygen. Sodium dithionite solution was made at a concentration of 100 mM in an anaerobic environment under nitrogen. 2 uL of 100 mM sodium dithionite was added to the 100 uM protein sample using an airtight syringe and mixed gently. The mixture was allowed to equilibrate for 5 minutes before taking the spectra. When the 409 nm peak remained, more sodium dithionite was added in 2 uL portions until there was no change in the protein spectra.

Metal Content Analysis

The identity of various transition metals bound to the protein was determined by Inductively Coupled Plasma-atomic emission spectrometry (ICP-AES) using the Optima

7000 DV spectrometer (PerkinElmer) in the Agricultural Diagnostic Service Center at the University of Hawaii.

Metal Reconstitution

Metal Reconstitution was done by stripping the protein of the bound metals and incorporating cobalt and iron according to the protocol commonly used for rubredoxins (Moura et al., 1991). 2 mg of pure protein was precipitated using 10% trichloroacetic acid (TCA) to a final concentration of 5% in the presence of 0.5 M β-mercaptoethanol (BME). The mixture was incubated at room temperature for about 5 minutes until all the protein precipitated. The colorless protein precipitate was collected by centrifugation at 8000 rpm for 5 minutes, and the supernatant was discarded. The protein pellet was dissolved in 0.5 M Tris-HCl, pH 8.0, containing 60 mM BME. The apoprotein at a concentration of 2 mg/mL was incubated at 4°C for 1 hour. $CoCl_2$ solution was added at an equimolar concentration to the protein, while ferrous ammonium sulfate solution was added at 5X the protein concentration. After 12 hours of incubation at 4°C, the samples were centrifuged at 8000 rpm for 5 minutes to remove undissolved/precipitated protein. The samples were purified on a Sephadex G-25 column (1 x 20 cm) equilibrated with 25 mM Tris HCI, 100 mM NaCl pH 8.0 buffer to remove the unbound metal.

Circular Dichroism Spectroscopy

Circular Dichroism (CD) was used to study the protein's secondary structure and thermal stability. The CD data were taken on a Chirascan v100 Spectrophotometer (Applied Photophysics). The protein samples were diluted to 0.1 mg/mL in 10 mM potassium phosphate buffer, pH 7.5, and the spectra were recorded in a quartz cell cuvette of 10 mm path length between 180 and 250 nm at 25° C with a bandwidth of 1.0 nm. The spectra were recorded in triplicate at a time constant of 1.0 s and averaged before subtracting the blank (buffer) spectrum. Thermal denaturation data was obtained by recording the ellipticity at 222 nm in 2°C intervals from 25 to 85 °C with a temperature increase of 1°C per minute.

Redox Potential

The redox potential of Rv1590 was determined by a spectrophotometric method employing a reducing system of sodium dithionite and methylene blue as a mediator(Vincent Massey, 1991). Redox potential experiments were done to determine how easily the iron atom could lose or gain electrons as compared to the know potential of the mediator dye. In a 1 mL cuvette, 2.5 uM methylene blue dye was mixed with a 90 uM protein sample in Tris–HCl buffer, at pH 8.0. The mixture was purged with nitrogen for 10 minutes to make it anaerobic. The UV-visible spectrum was scanned from 200 nm to 900 nm, representing the oxidized state for both the protein and the dye. 2 uL of 1 mM sodium dithionite was added to the protein-dye mixture through an airtight syringe. The mixture was stirred, and the spectrum was recorded after 2 minutes. More sodium dithionite was added at 2 uL intervals until there was no further change in the spectrum.

The spectra (wavelength vs. absorbance) were transferred from the spectrophotometer into an excel spreadsheet for analysis

CHAPTER 3: RESULTS AND DISCUSSION

Bioinformatics

A BLAST search for homologs of Rv1590 using standard parameters yields 2552 homologous sequences, all found in Actinobacteria. To speed further analysis, the top 100 homologs were examined using BLAST sequence alignment tools. The 100 homologs of Rv1590 obtained had percent identities between 56.8 and 100, with sequence lengths ranging from 49 to 200 amino acids. All the homologs belong to the gram-positive actinobacteria (Figure 7).

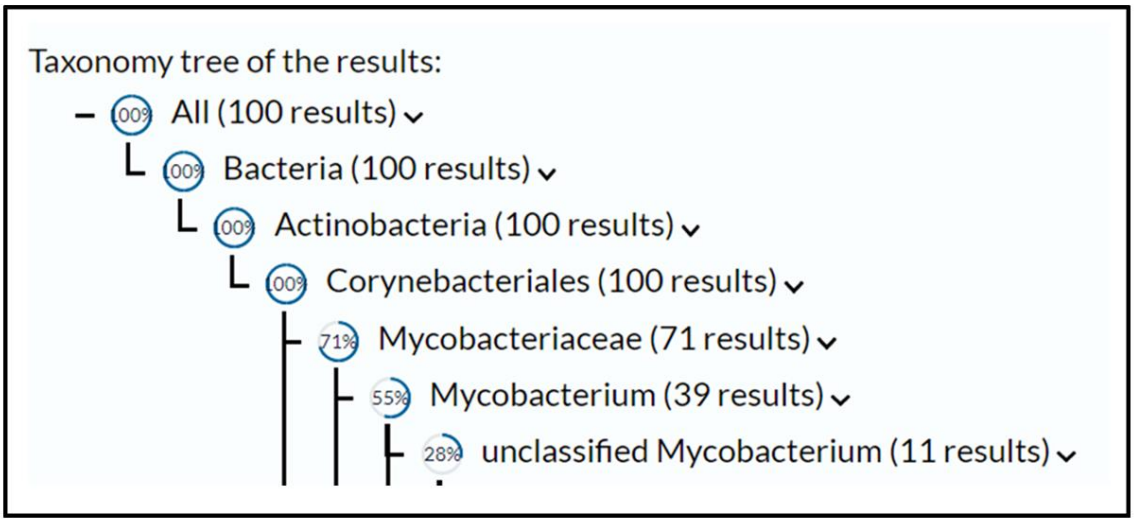

Figure 7. Taxonomy distribution of the 100 homologs of Rv1590.

Alignment of the 100 homologs reveals 21 conserved amino acids with sequence variation observed in the N-terminus (Figure 8). Figure 9 shows the distribution of the

conserved amino acid residues in the Rv1590 sequence. The alignment of nine rubredoxins sequences, with solved crystal structures, and Rv1590, shows seven conserved residues in Rv1590 (Figure 10). The conserved residues include three cysteines, a proline, a tryptophan, and two glycine residues. In Rv1590, the metal is coordinated by the three cysteines and one histidine, while in the other rubredoxins, metal coordination is by four cysteines.

```
A0A5N5VAN0|A0A5N5VAN0_MYCPH      -----------------------------------MAFNVYTGE-PDGT----EVPTAA      19
G7CAV0|G7CAV0_MYCT3              -----------------------------------MYNVYTGE-PEGG----PTPPAA      18
A0A2A7MZG5|A0A2A7MZG5_MYCAG      --------------------------------MGTAKFNVYTGE-PAGG----DVPTAA      22
A0A1A1Y703|A0A1A1Y703_9MYCO      ---------------------------------MAAKFNVYTGE-PAGG----ADPTAA      21
A0A2S8K9Q1|A0A2S8K9Q1_9MYCO      ----------------------------MVSPDGTAKFNVYTGE-PAGG----AVPTAA      26
                                                                   :. .**           * .*

A0A5N5VAN0|A0A5N5VAN0_MYCPH      RLGLEPPRFCADCGRRMVVQVRPDGWSATCSRHGTTDSKDLELR-      63
G7CAV0|G7CAV0_MYCT3              QLGLEPPRFCAECGRRMVVQVRPDGWSAKCSRHGVIDSADLEPYR      63
A0A2A7MZG5|A0A2A7MZG5_MYCAG      QLGLEPPRFCAECGRRMVVQVRPDGWSAKCSRHGVQDSKDLEDKR      67
A0A1A1Y703|A0A1A1Y703_9MYCO      QLGLEPPRFCAECGRRMVVQVRPDGWLAKCSRHGEQDSKDLDERR      66
A0A2S8K9Q1|A0A2S8K9Q1_9MYCO      QLGLEPPRFCAECGRRMVVQVRPDGWSARCSRHGTQDSKDLDER-      70
                                  :***  *:*  ***:* **: * **   *:**.   :
```

Figure 8. BLAST alignment results of 100 homologs. Only five sequences are shown to highlight the conserved residues. The alignment is denoted using the ClustalW format where '*' indicates a fully conserved residue, ':' indicates conservation of residues with strongly similar properties, and '.' indicates conservation of residues with weakly similar properties.

Rv1590 has a phenylalanine residue adjacent to the first cysteine ligand, whereas, in the other rubredoxins, this corresponding position has either tryptophan or tyrosine residue. Rv1590 also has two consecutive tryptophan residues at positions 60 and 61 and an alanine residue at position 62. The conserved hydrophobic residues have been

shown to form a hydrophobic core contributing to the stability of the protein structure and the two loops holding the iron atom structure (Sieker et al., 1986)

```
1                                                                   40
M V E I V A G K Q R A P V A A G V Y N V Y T G E L A D T A T P T A A R M G L E P

41                                                                  79
P R F C A Q C G R R M V V Q V R P D G W W A R C S R H G Q V D S A D L A T Q R
```

Figure 9. The amino acid sequence of Rv1590.The red and blue-colored residues are conserved in the 100 homologs. The metal-coordinating residues are shown in red.

```
A.calcoaceticus      MKKYQCIVCGWIYDEAEGWPQDGIAAGTKWEDIPDDW--TCPDCGVSKADFEMIEI-
P.aeruginosa         MRKWQCVVCGFIYDEALGLPEEGIPAGTRWEDIPADW--VCPDCGVGKIDFEMIEIA
P.furiosus           MAKWVCKICGYIYDEDAGDPDNGISPGTKFEELPDDW--VCPICGAPKSEFEKLED-
P.abyssi             MAKWRCKICGYIYDEDEGDPDNGISPGTKFEDLPDDW--VCPLCGAPKSEFERIE--
D.vulgaris           MKKYVCTVCGYEYDPAEGDPDNGVKPGTAFEDVPADW--VCPICGAPKSEFEPA---
M.gigas              MDIYVCTVCGYEYDPAKGDPDSGIKPGTKFEDLPDDW--ACPVCGASKDAFEKQ---
C.pasteurianum       MKKYTCTVCGYIYNPEDGDPDNGVNPGTDFKDIPDDW--VCPLCGVGKDQFEEVEE-
C.perfringens        MKKFICDVCGYIYDPAVGDPDNGVEPGTEFKDIPDDW--VCPLCGVDKSQFSETE--
D.desulfuricans      MQKYVCNVCGYEYDPAEHDN-------VPFDQLPDDW--CCPVCGVSKDQFSPA---
Rv1590               EPPRFCAQCGRR--------------MVVQVRPDGWWARCSRHGQVDSADLATQR-
                          *  **                   .  * .*   *.  *  .
```

Figure 10. ClustalW multiple sequence alignments of Rv1590 and known rubredoxins from different organisms. All the rubredoxins have complete sequences shown, while residues 1-38 are truncated in Rv1590. '*' indicates a fully conserved residue. '.' indicates the conservation of amino acids of weakly similar properties.

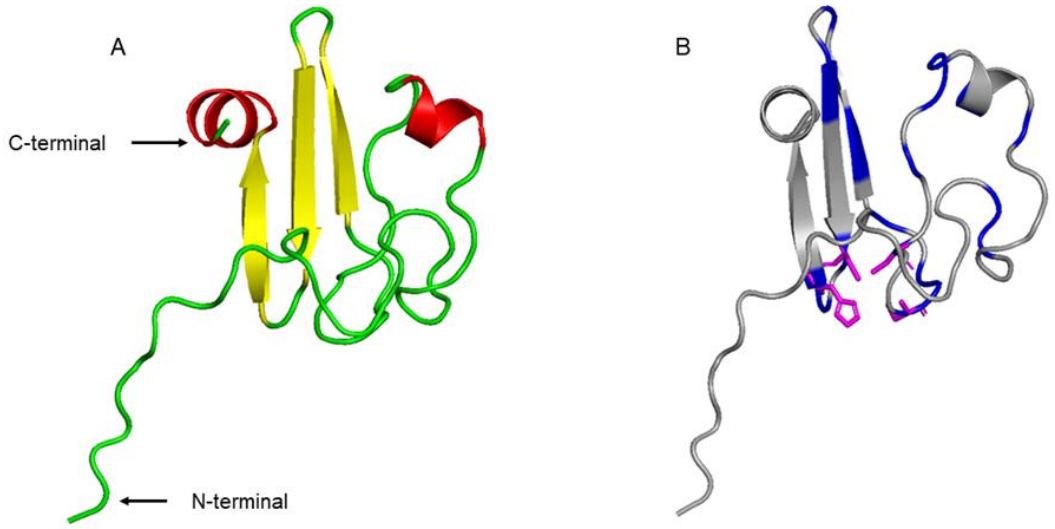

Figure 11. The predicted secondary structure of Rv1590 is illustrated in PyMOL. **(A)** Beta sheets, alpha helices, and random coils are shown in yellow, red, and green, respectively. **(B)** Conserved residues and metal ligands represented as sticks are shown in blue and magenta, respectively.

The three-dimensional (3D) structures of rubredoxins belong to the α+β class, with 2 α-helices and 2-3 β-strands (Sieker et al., 1986). Due to the lack of a solved crystal structure, studies involving the 3D structure of Rv1590 can only be based on the predicted structure. Figure 11 shows the 3D structure of Rv1590 predicted by AlphaFold, an artificial intelligence algorithm that predicts the 3D structure of the protein from its amino acid sequence using either available protein structures as templates or multiple sequence alignment (Jumper et al., 2021). The predicted structure for Rv1590 has a fold similar to the characterized rubredoxin B (Rv3250c) from *Mycobacterium tuberculosis* (Buchko et al., 2011) consisting of one antiparallel β-sheet with three strands connected by two

loops. The first pair of metal ligands, one cysteine and histidine, are located at the N-terminal end of the first β-strand, the second pair of metal ligands (two cysteines) are located on the loop connecting the second and third β-strands (Figure 11 A). Figure 11B also highlights the residues conserved in the 100 homologs showing their distribution throughout the protein structure except for the most variable N-terminus.

Table 7. pLDDT scores of the different regions of RV1590 predicted structure

Residues	**pLDDT score**	**Region**
1-7	<50	Unstructured
8-10	50-70	Unstructured
11-16	70-90	Unstructured
17-73	>90	Unstructured, alpha helix and beta sheets
74-79	50-80	Alpha helix

AlphaFold prediction produces a per-residue estimate (pLDDT score) on a 0-100 scale. Regions with pLDDT > 90 are expected to be modeled with high accuracy, pLDDT between 70 and 90 represent regions expected to be modeled with a generally good backbone prediction, and regions modeled with low confidence have pLDDT between 50 and 70 and should be treated cautiously. Regions with pLDDT < 50 are often disordered, either unstructured or only structured as part of a complex and should not be interpreted. Table 7 shows the pLDDT scores of the different regions of Rv1590 as predicted by AlphaFold, with the segment composed of residue 17 to 73 having the highest prediction

accuracy. This protein segment contains all the conserved residues, including the metal ligands.

Molecular Cloning

The Rv1590 gene was cloned and overexpressed in *E. coli*. The gene and the pETHSUL vector were amplified by PCR and confirmed by agarose gel electrophoresis. The PCR products of the pETHSUL vector and Rv1590 were visualized on an agarose gel as single bands close to their 5677 bp and 260 bp sizes, respectively (Figure 12A). The plasmid was digested by HindIII and BamHI enzymes (Figure 12B) to confirm the enzymes' efficiency before cloning. Digestion results in the linearization of the plasmid generating a 5.6 kb linear plasmid shown in lanes 3. The undigested plasmid is circular, supercoiled, and compact and travels faster than the linear plasmid of the same size; therefore, it is observed at 4 kb in lane 2.

The pETHSUL vector was treated with thermostable alkaline phosphatase (TSAP) during restriction enzyme digestion. TSAP is used in molecular biology to catalyze the dephosphorylation of the 5' and 3' ends of the DNA generated after digestion. TSAP catalyzed the dephosphorylation at both ends of the linearized pETHSUL vector generated after restriction enzyme digestion to prevent religation. Religation of the vector to itself would hinder the ligation of the gene into the vector. The concentrations were determined, and ligations were set up as mentioned in Materials and Methods. Enough colonies were observed when the ligation product was transformed into the *E. coli* competent cells and grown on an ampicillin-selective LB plate. The purified recombinant

DNA was confirmed to contain the Rv1590 gene using the PCR reaction discussed in the methodology (the PCR result was similar to figure 12A, lane 2).

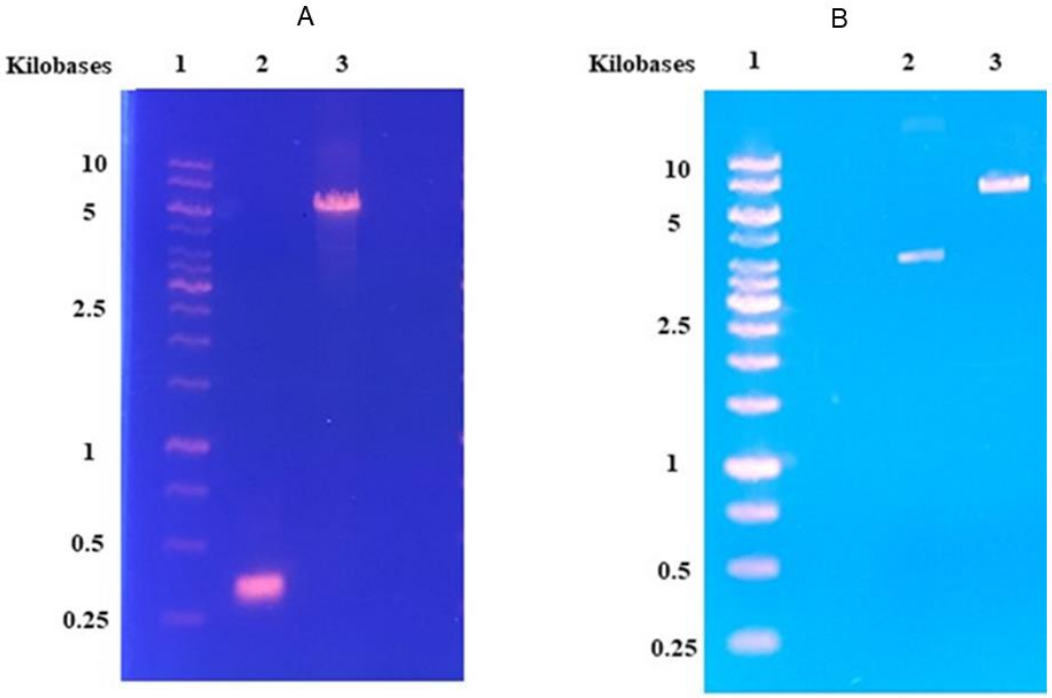

Figure 12. Agarose gel of PCR products. A) The lanes correspond to the 1kb DNA ladder (Lane-1), Rv1590 (Lane 2), and pETHSUL (Lane-3). B) Agarose gel of restriction digestion of pETHSUL plasmid.1kb DNA ladder (Lane-1), uncut pETHSUL plasmid (Lane-2), cut pETHSUL plasmid (Lane-3).

Protein Expression and Purification

Expression of rubredoxins in native organisms usually results in low yield and expression in *E. coli* using minimal media significantly improves the yield. One advantage of purification from the native host is the incorporation of the correct metal ion. Binding the correct metal ions into metalloproteins sometimes requires special protein machinery

and chaperones (Hausinger, 1990), which may be absent in *E. coli*. Thus, a recombinant expression of rubredoxins in *E. coli* does not always result in holo proteins with correct metal bound in the optimum amount. Also, metal insertion depends on the amounts of available metal ions in the medium (Hausinger, 1990). Therefore, an excess of ferrous ions was added to the minimal media during expression to achieve full metal incorporation. It was also evident that different growth conditions resulted in different amounts of iron bound to the protein. LB media without ferrous ions added produced the least amount of metal, while minimal media supplemented with ferrous ions produced the highest amount of iron bound to the protein (Figure 18).

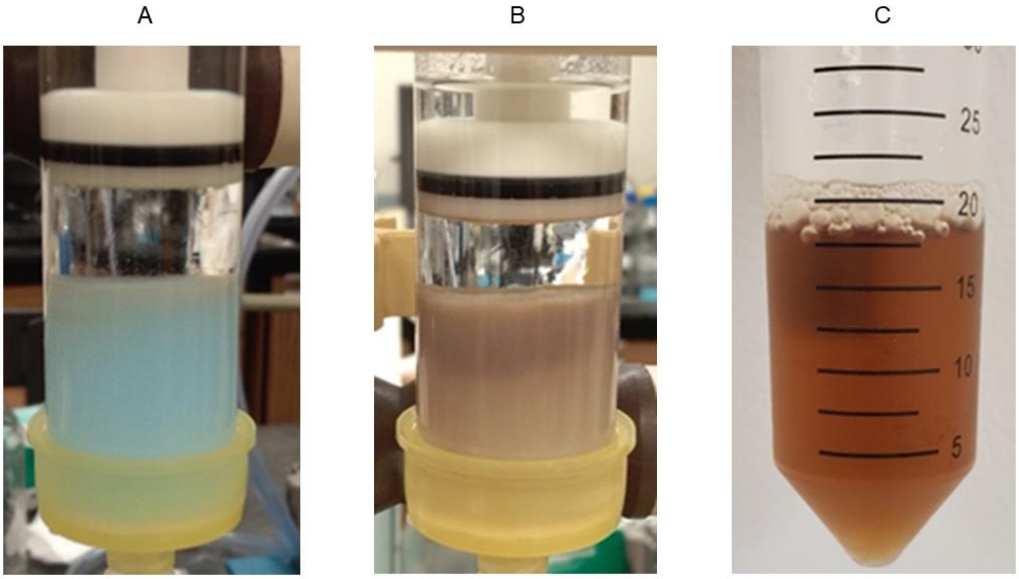

Figure 14. A) The Ni-NTA column before protein binding. **B)** The Ni-NTA column after Rv1590 is bound to the resin. **C)** The eluted protein.

The SDS PAGE for the small-scale expression of Rv1590 is shown in Figure 15. The pETHSUL vector without Rv1590 shows the expression of the SUMO protein at ~15

kDa and no expression of the protein of interest. SUMO-Rv1590 has a calculated size of 20.8 KDa, however, it is observed at about ~ 25 kDa on the gel. Studies have shown that SUMO can be detected in a range of ~18 to 28 kDa.

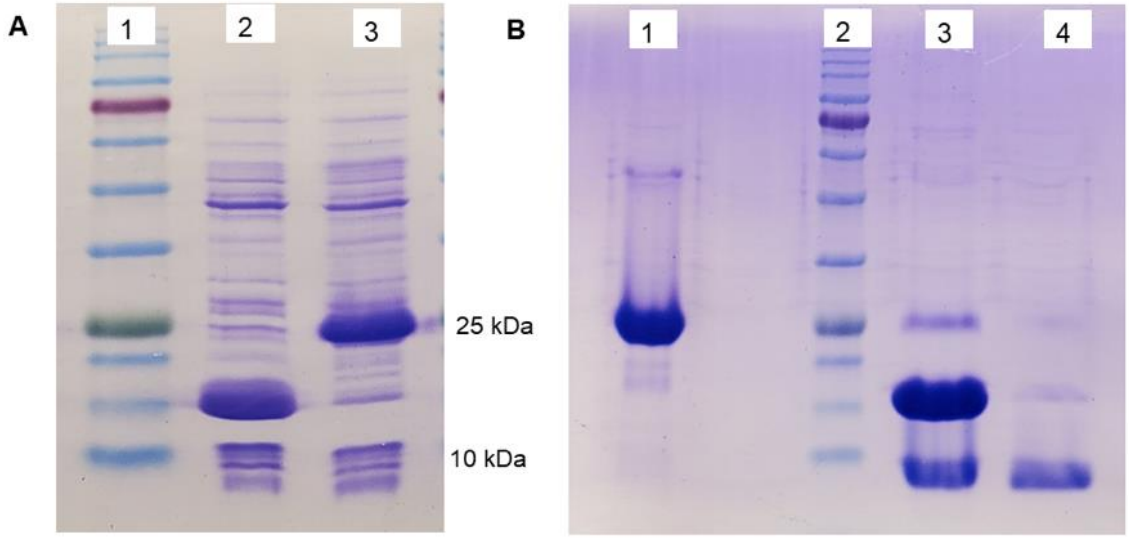

Fig. 15. SDS-PAGE gels (**A)** Small scale expression. Molecular weight standard (lane 1), pETHSUL vector without Rv1590 (lane2) and pETHSUL vector plus Rv1590 (lane 3). **(B)** Cleavage of SUMO-Rv1590. Uncleaved Rv1590-SUMO (lane 1), molecular weight standard (lane 2), cleaved SUMO-Rv1590 (lane 3), pure Rv1590 (lane 4).

The protein was purified using Immobilized Metal Affinity Chromatography (IMAC). After cell lysis and centrifugation, the cleared lysate was loaded onto an equilibrated Ni-NTA column. Figure 14 shows the color change that occurred when a significant amount of the protein was loaded onto the Ni-NTA column. The column was washed with a buffer containing a low concentration of imidazole (5 mM) to remove loosely and nonspecifically bound proteins. Finally, the bound protein was eluted with a high-concentration imidazole

buffer. The eluted protein had an intense brown color due to the absorbance of UV light by the bound ferric ions (Figure 14). The purity of the eluted was analyzed by SDS-PAGE.

Protein quantitation was conducted using absorption at 280 nm of the denatured protein, and the theoretical extinction coefficient of 15470 $M^{-1}cm^{-1}$ calculated using ExPASy. About 70 mg of protein was purified per liter of cell culture. Overnight cleavage of the purified Using a 1:1000 (SUMO protease: protein) mass ratio was sufficient to cleave the fusion protein releasing the mature protein (Figure 15). The pure protein obtained from the cleavage was colorless, indicating the loss of the originally bound ferric iron. The protein was judged pure from the SDS-PAGE analysis, and no further purification step was necessary.

Protein Characterization

UV-Vis Spectroscopy

Ultraviolet-visible spectroscopy (UV-Vis) probes the electronic state of a compound using light in the ultraviolet to visible range, 180 – 380 nm, and 380 – 750 nm, respectively (Hughes & Krauszat al, 2011). Biomolecules contain functional groups capable of absorbing light and getting excited from the group state to a higher energy state, thus giving out characteristic spectra (Perkampus, 1992). Absorption bands can appear either at lower or higher wavelengths signifying higher and lower energy requirements for the transition from the ground state to the excited state. All proteins have a UV-Vis spectrum due to their amide backbone, which absorbs light at ~215 nm, and aromatic amino acids present in some proteins, which absorb light at ~280 nm light.

Metalloproteins have additional absorption bands due to charge transfer from electrons in the orbitals on either the metal or ligand transferring to low-energy unoccupied orbitals on the ligand (metal-to-ligand) or metal (ligand-to-metal), MLCTs, and LMCTs, respectively.

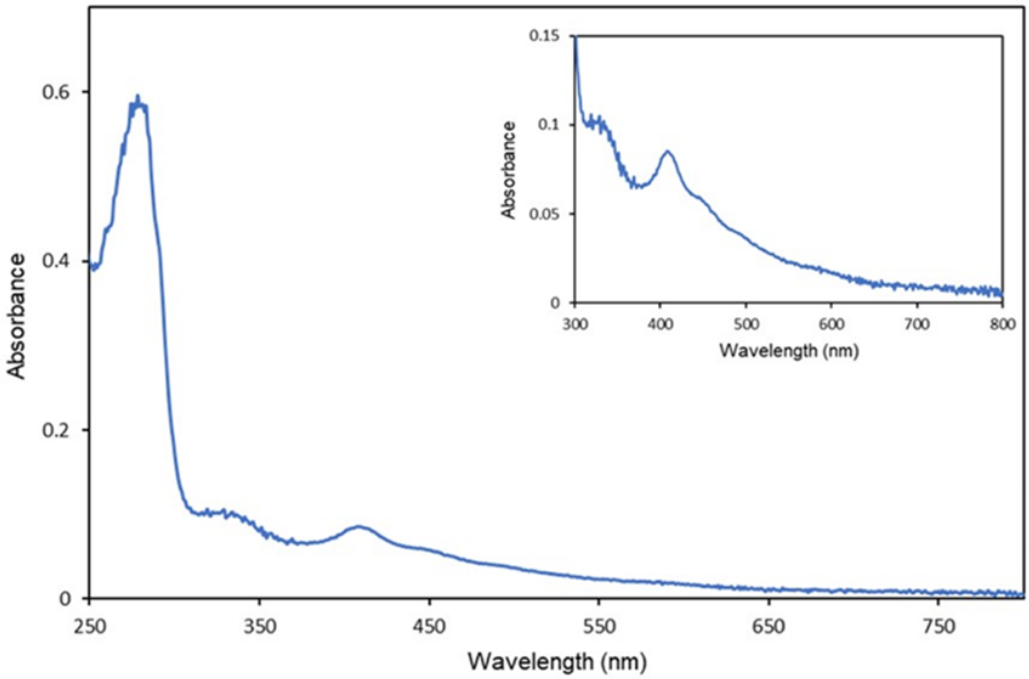

Figure 17. UV-Visible absorption spectra of oxidized Rv1590. The insert is a zoom-in of the bands.

Oxidized rubredoxins have a brown-reddish color and display UV-Vis absorption bands at 280,350, 380,490,570, and 750 nm, while reduced rubredoxins are colorless with absorption bands at 315 and 330 nm (Lovenberg & Sobel, 1965). The electronic absorption spectrum of the Rv1590 (Figure 17) has absorption bands at 280,330, and 410 nm with overlapping bands at 450, 495, and 600 nm. The band at 280 nm is due to

the polypeptide's aromatic residues, tyrosine, and tryptophan. The rest of the bands likely result from ligand-to-metal charge transfer (LMCTs) associated with a cysteinyl-ligated iron. The 410 nm absorption feature in the spectrum of RV1590 is due to cysteine – Fe (III) LMCT, whereas the band at 330 nm may result from cysteine – Fe (II) LMCT (Gupta et al., 1995). The UV-Visible spectrum of the protein expressed LB, or minimal media, shows that the highest amount of iron is bound in the iron-supplemented minimal media based on the intensity of the peaks at 410 nm (Figure 18).

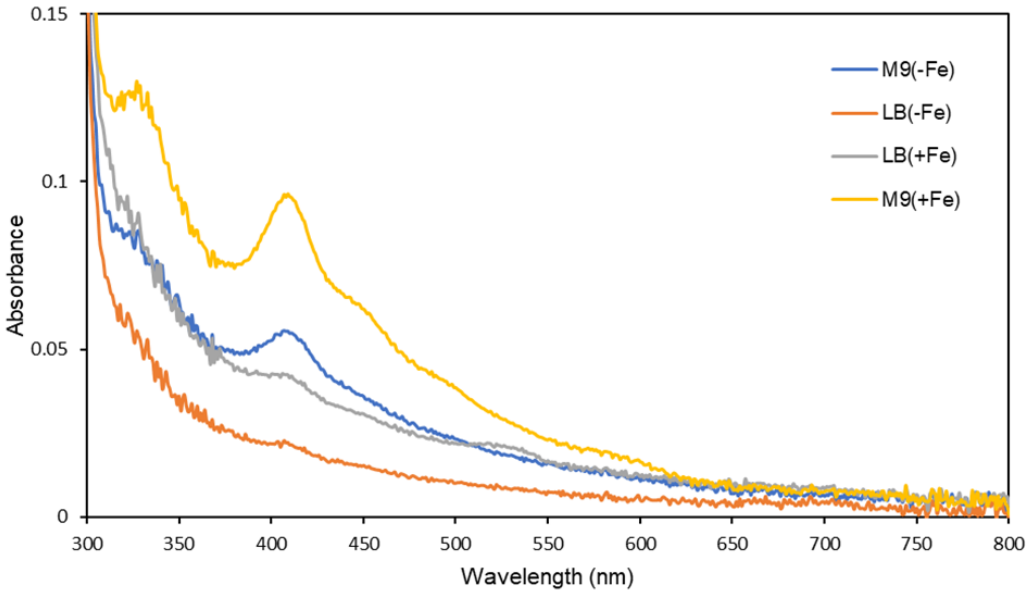

Figure 18. The electronic absorption spectra of the SUMO-Rv1590 purified from different expression media. M9(-Fe) (minimal media without iron), M9(+Fe) (minimal media with iron), LB(-Fe) (LB without iron) and LB(+Fe) (LB with iron)

Molecular Mass Determination

The molecular mass of the pure Rv1590 was determined using electrospray ionization mass spectrometry (ESI–MS). ESI–MS generates highly charged ion species of peptides or proteins by protonation (positive ion mode) or deprotonation (negative ion mode) (Fenn et al., 1989). The ions are accelerated in an electric or magnetic field to the mass analyzer and displayed as a spectrum of multiple peaks that differ only in the number of protons attached. The peaks in the spectrum are used to calculate the average mass of the protein with the assumption that (i) adjacent peaks differ by one charge and (ii) charging is due to the same species (e.g., proton H+). In this project, positive ion mode was used, and the spectrum in Figure 16 was obtained for Rv1590.

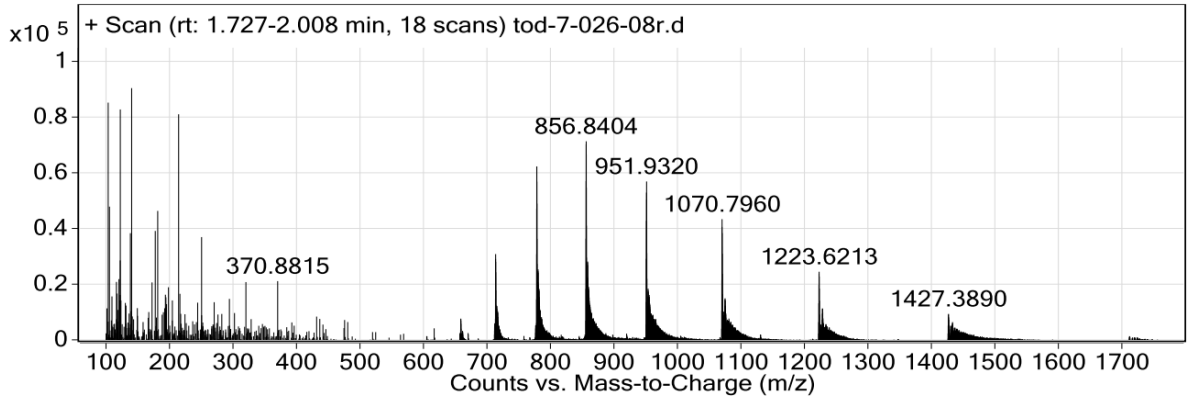

Figure 16. Electrospray ionization mass spectrum of Rv1590

The molecular mass of Rv1590 was calculated from two adjacent peaks. Before calculating the protein's mass, each peak's charge state must be determined.

$$Z_1 = (M_2 - 1.0079)/(M_2 - M_1)$$

M_1 and M_2 are the m/z values of two adjacent peaks in the mass spectrum ($M_2>M_1$). Z_1 is the charge of M_1, and 1.00079 is the mass of a proton in Da.

$$Z_1= (951.9320-1.0079)/(951.9320-856.8404)$$

$$Z_1 = 10$$

$$Z_2=Z_1-1$$

The number 1 indicates the difference in charge between the two adjacent peaks, assuming the peaks are from the same compound and differ by only one charge.

$$Mass = Z_1(M_1-1.0079)$$

$$Mass = 10(856.8404-1.0079)$$

$$Mass = 8558.3250 \text{ Da}$$

Table 20. The experimental mass calculation for Rv1590

M_2	M_1	M_2-M_1	Z_1	Experimental mass
1223.6213	1070.7960	152.8253	8.0001	8558.3048
1070.7960	951.9320	118.8640	9.0001	8558.3169
951.9320	856.8404	95.0916	10.0001	8558.3250
Average mass				**8558.3156**

Table 20 shows the experimental mass calculated using three sets of adjacent peaks and the average mass. The charge of each peak increases by one unit from high to low mass (Table 20), assuming that the ionizing species is a proton with a nominal mass of 1 Da, indicating that the peaks are from the same peptide and not due to impurities or contaminant peptides. The average experimental molecular mass was 8558.3156 Da, which is in good agreement with the 8558.72 Da calculated from the amino acid sequence using ExPASy.

Metal Content Analysis

Metal ion contamination is common during the expression, purification, and handling of metalloproteins. A major contaminant is zinc due to its large quantities in cells and presence on most surfaces. Divalent metals have different binding affinities to metalloproteins, with Mg^{2+} and Zn^{2+} having the lowest and highest affinities, respectively. The order of binding affinities is represented as the Irving–Williams series: (Mg^{2+} and Ca^{2+} (weakest binding) < Mn^{2+} < Fe^{2+} < Co^{2+} < Ni^{2+} < Cu^{2+} > Zn^{2+}) (Irving & Williams, 1948).

Metal concentration in the purified protein solution was determined using inductively coupled plasma mass spectrometry (ICP-MS) (Wilschefski & Baxter, 2019). Metal analysis of purified Rv1590 showed that metals other than iron were bound to the protein (Table 21). Studies have shown that metals that prefer tetrahedral coordination, such as Fe, Co, Zn, Ga, and Cd, bind to the metal coordination site of rubredoxin with similar geometries (Holm et al., 1996). A mixture of iron and zinc forms is obtained when rubredoxins are overexpressed in *E. coli,* and a study using electrospray ionization

Fourier transform ion cyclotron resonance (ESI-FTICR) mass spectrometry showed that iron and zin bounding in rubredoxins occurs simultaneously but at different rates during overexpression in *E. coli* (Taylor et al., 2001). However, the mechanisms for selective iron incorporation over zinc into rubredoxin in native organisms remain unknown.

Table 21. Metal analysis of Rv1590 in minimal media and purified using Ni-NTA column

Percent composition					
	Cu	Co	Fe	Ni	Zn
Sample 1	9.6	1.9	26.4	38.2	23.4
Sample 2	9.1	1.9	25.1	39.1	24.6

The iron-plus-zinc contents make up for ~ 64% of the metals bound to Rv1590 (Table 21). According to the Irving- Williams series, all the metals in table 21 have higher binding affinities than iron. Nickel can be traced to contamination from the Ni-NTA column during purification. Cases have been reported of iron loss during rubredoxin purification; hence it's possible that the empty binding sites in Rv1590 due to iron loss became occupied by nickel from the column.

Metal Reconstitution

As discussed previously, Rv1590 was purified with other metals other than iron bound to the protein even though the media was supplemented with excess iron. A study by Archer *et al.* on the structures of metal-substituted forms of the rubredoxin-like protein desulforedoxin from *Desulfovibrio gigas* revealed that rubredoxins can bind transition metals other than iron with no effect on the secondary and tertiary structure regardless of the metal incorporated (Archer et al., 1999).

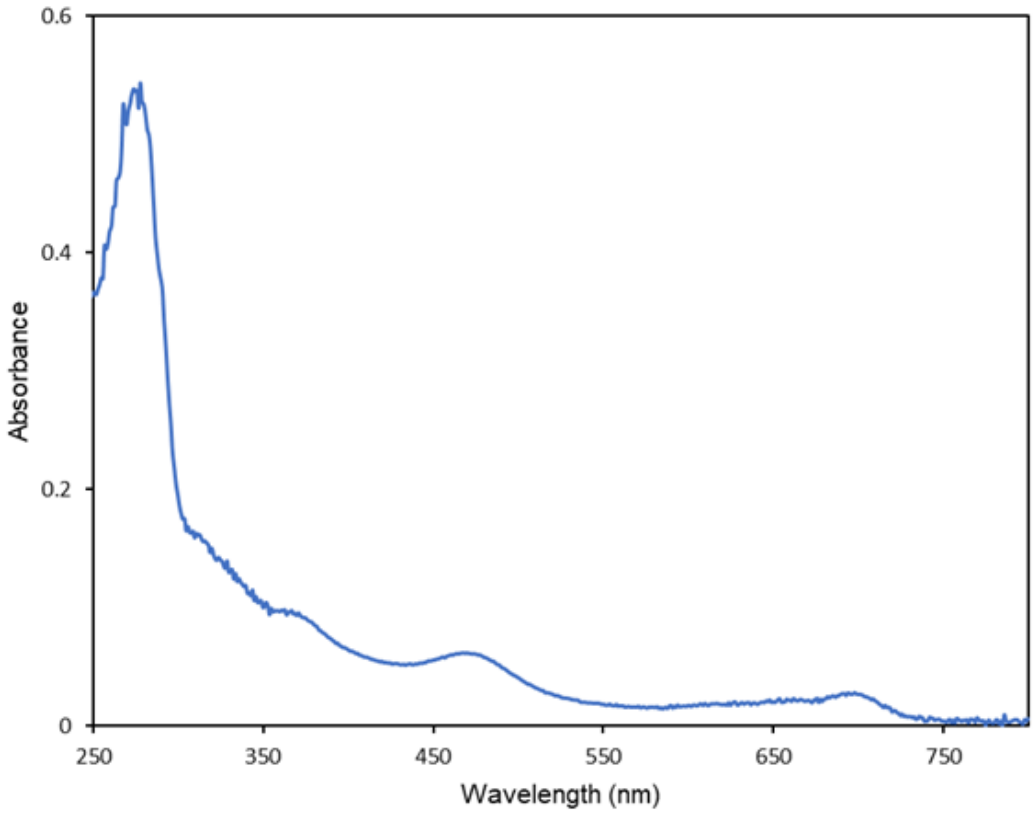

Figure 19. The UV-visible electronic absorption spectrum of cobalt substituted Rv1590

Metal reconstitution was done to remove the bound metal ions to generate apo-protein, and iron and cobalt were incorporated. Metal reconstitution was done by denaturation of the protein in the presence of trichloroacetic acid, followed by refolding and incubating the protein with the desired metal. Incorporating metal ions into the apo-protein was done by adding small amounts of the final metal concentration stepwise while stirring the protein to avoid protein precipitation, denaturation, and aggregation. Ferrous ions could be added at five times the protein concentration without precipitation. However, cobalt at a concentration three times the protein concentration caused protein precipitation. After adding metal ions at the desired concentration, the samples were incubated for 12 hours to ensure the complete incorporation of the metal into the protein. The time needed for metal incorporation depends on the protein binding kinetics and can be seconds, minutes, or hours. This project did not determine the time for metal incorporation into Rv1590, and 12 hours was chosen arbitrarily.

The cobalt-substituted rubredoxin exhibit three bands at 360, 470, and 700 nm in the UV-vis spectrum (Figure 19). The bands at 360 and 470 nm originate from charge transfer transitions from the bound ligands to Cobalt (II). The low-intensity band at 700 nm originates from d-d ligand field transitions (May & Kuo, 1978). The UV-vis spectrum of iron reconstitution Rv1590 has absorption bands at 280 and 330 nm (Figure 20), representing the reduced protein. Attempts to get oxidized Rv1590 by exposing the reduced protein to air or using Fe (III) in the reconstitution were unsuccessful.

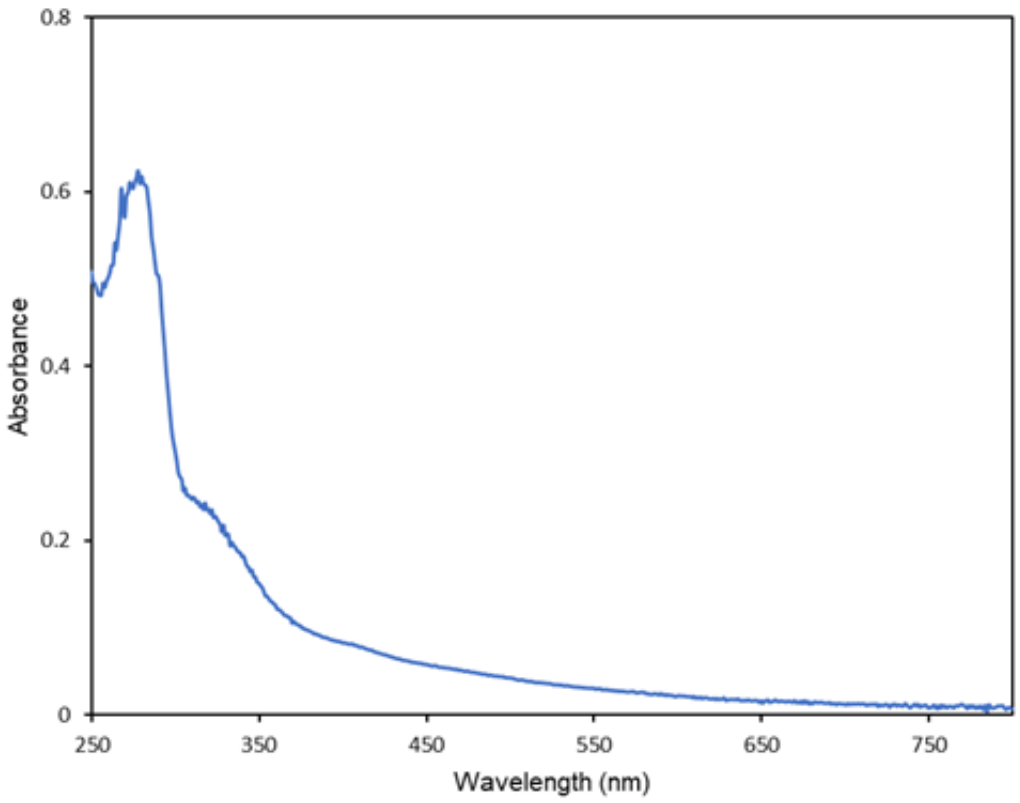

Figure 20. The UV-visible electronic absorption spectrum of iron substituted Rv1590

Circular Dichroism Spectroscopy

Circular dichroism (CD) is a technique used for the determination of the secondary structure of proteins in the far ultraviolet range (178 to 260 nm) and to monitor protein-bound cofactors (prosthetic groups) such as metal ions, iron-sulfur clusters, hemes, or flavins in the near ultraviolet range (300 to 600 nm) (Kelly & Price, 2000). CD spectrum in the far UV is derived from the protein amide backbone, which is sensitive to the secondary structure (Josephet al., 2001). Different structural elements have characteristic CD spectra. α-helical proteins have minima at 222 nm and 208 nm and a maximum at

195 nm. β-pleated sheets have a minimum at 218 nm and a maximum at 195 nm (Greenfield, 2006).

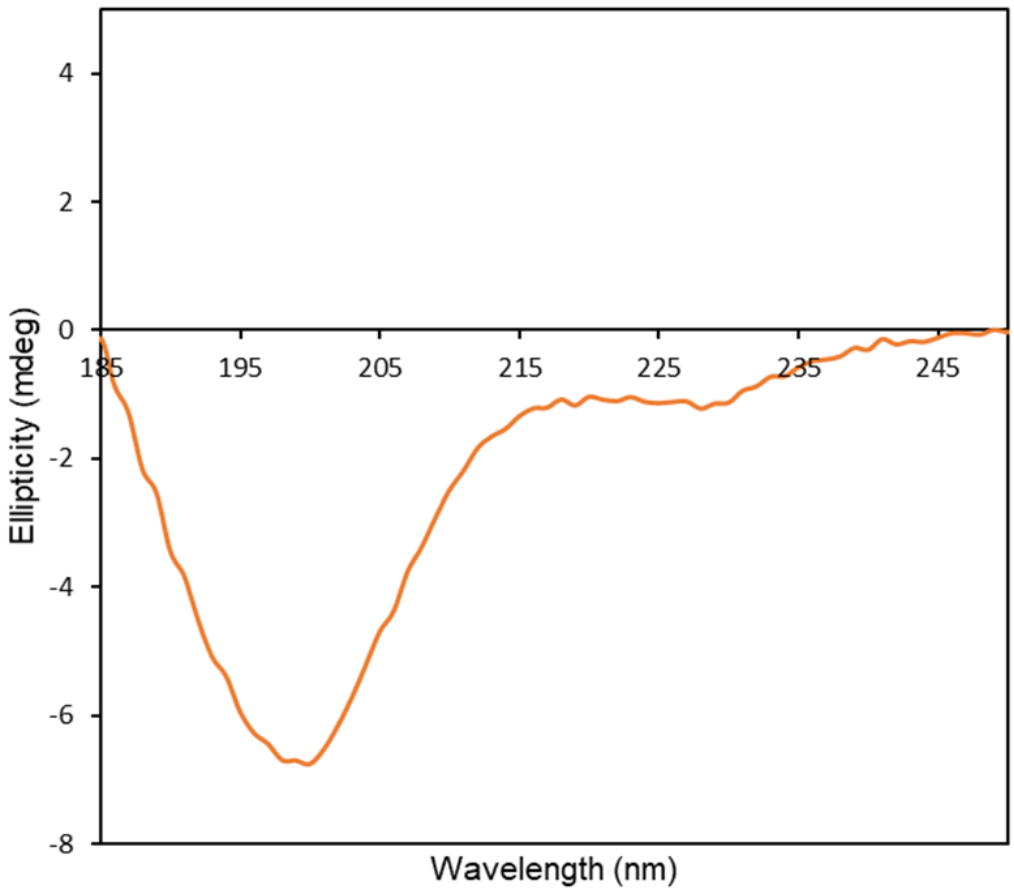

Figure 21. Far-UV CD spectrum of the Rv1590 collected at 25 °C.

The far-UV CD spectrum of holo-rubredoxins is characterized by a double minimum at 204 nm and 227 nm (Buchko et al., 2011). The 204 nm band is due to a combination of random coil and polyproline type II (PPII) structure, while the 225 nm band results from a combination of b-sheet and the excited state-induced CD transitions

aromatic residues clustered together within the protein's core. CD spectrum of Rv1590 (Figure 21) is characterized by two negative bands at 226 and 200 nm. The band at 200 nm is due to random coils which may also be attributed to the protein existing in unfolded state at the specific experimental conditions.

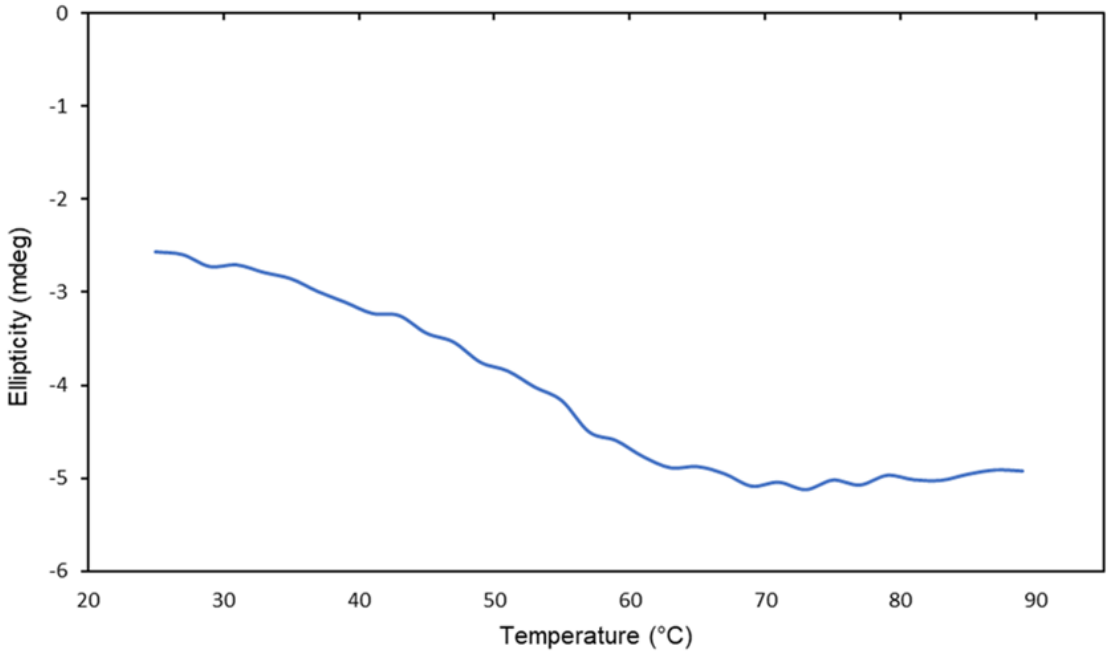

Figure 22. The CD thermal plot for Rv1590 was obtained by measuring the ellipticity at 226 nm between 25 °C and 90 °C.

Rubredoxins are very stable proteins. RubB from *M. tuberculosis* is stable up to 85° C (Buchko et al., 2011), and rubredoxin from *Pyrococcus furiosus* has a melting temperature of 144 °C (LeMaster et al., 2004). Rv1590 was unstable right from 25° C (Figure 22). The observed low stability may be due to the protein existing in unfolded or unstructured state at the experimental conditions. The absence of metal ion in the active

site as the metal is lost during the cleavage of the fusion protein may be another plausible explanation for the low stability if the metal is needed for the protein's stability. Thermal denaturation of cobalt and iron substituted Rv1590 gave similar thermal stability results. However, the metal substituted Rv1590 in this project may not be used as a reference because metal analysis was not done to confirm that the protein was fully loaded with the metal.

Sodium Dithionite Reduction

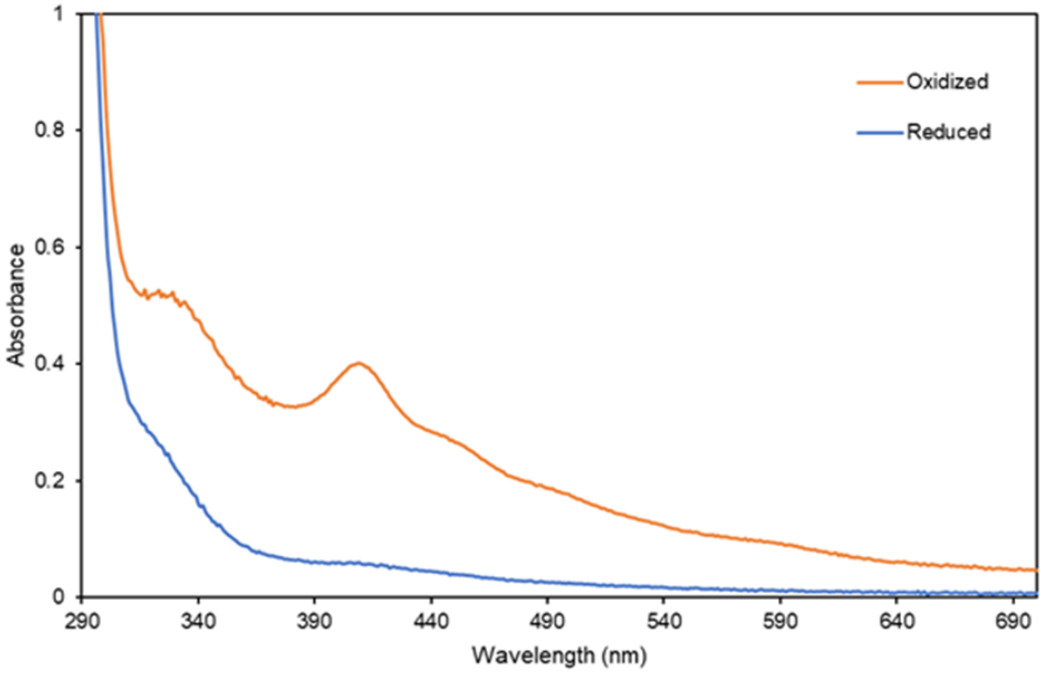

Figure 23. UV-visible electronic spectrum of anaerobic reduction of Rv1590 by sodium dithionite.

Sodium dithionite ($Na_2S_2O_4$) solution contains $SO_2^{\bullet-}$, which acts as a reductant. Electron carriers such as metalloproteins are reduced by the radical $SO_2^{\bullet-}$ through successive one-electron transfer reactions (Mayhew & Massey, 1973) as shown below.

$$SO_2^{\bullet-} + P \rightarrow SO_2 + P^-$$

P and P^- are the protein's oxidized and reduced forms. Oxidized Rv1590 was converted to the reduced form using sodium dithionite as the reductant in an anaerobic environment. The reduction of Rv1590 was monitored by observing the loss of the 410 nm peak absorbance (Figure 23).

Redox Potential

The reduction potential (E_m) measures the thermodynamic tendency of a redox center to accept or donate an electron(s) and is traditionally expressed relative to the Standard Hydrogen Electrode (SHE) defined with E_m = 0 mV. In a reaction involving two redox centers, the center with the lowest E_m value will serve as the electron donor, whereas the center with the more positive E_m value will act as the electron acceptor. The reduction potentials of homologous proteins with the same prosthetic group can vary by hundreds of millivolts even though the redox sites are highly similar (T. E. Meyer et al., 1983; Moura et al., 1979). The electrostatic environment, hydrogen bonding of the redox center, and the degree of solvation are the main determinants of the reduction potential (Gámiz-Hernández et al., 2009; Stillman, 2007).

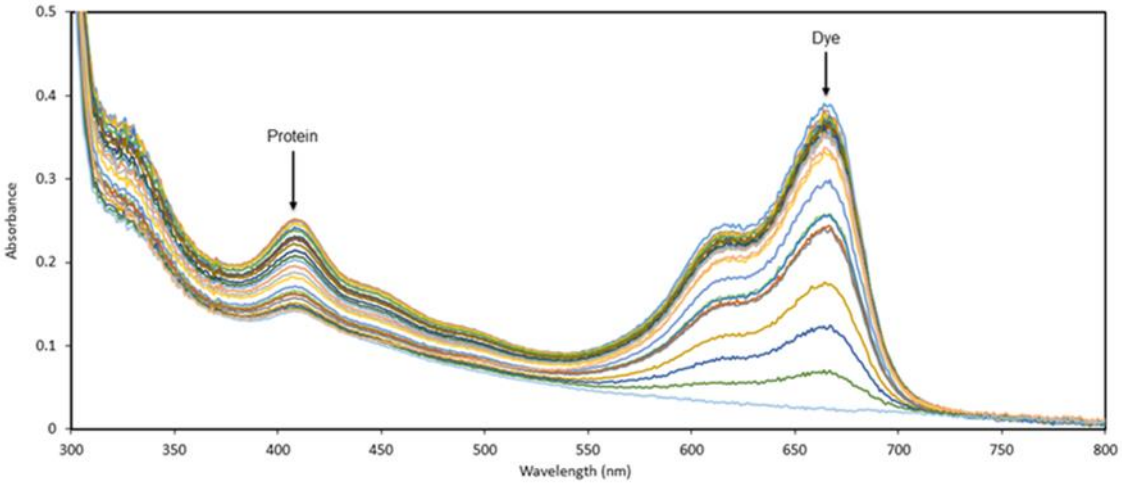

Figure 24. The UV-visible electronic spectrum of anaerobic determination of the redox potential of Rv1590 using sodium dithionite and methylene blue

The reduction potential of Rv1590 was determined using methylene blue, which served as a reference dye of known redox potential, and sodium dithionite as a reductant. The dye should have a redox potential of 30 mV within the redox potential of the protein. Also, the spectral absorbance of the dye and protein should have no interference with each other. Methylene blue has a redox potential of –4 mV at pH 7.5 (Clark et al., 1925) and its maximum absorption band at 665 nm does not interfere with the protein's absorption band at 410 nm. The anaerobic protein-dye mixture was reduced with sodium dithionite stepwise, and reductions of the dye and protein were monitored at 410 and 665 nm, respectively (Figure 24).

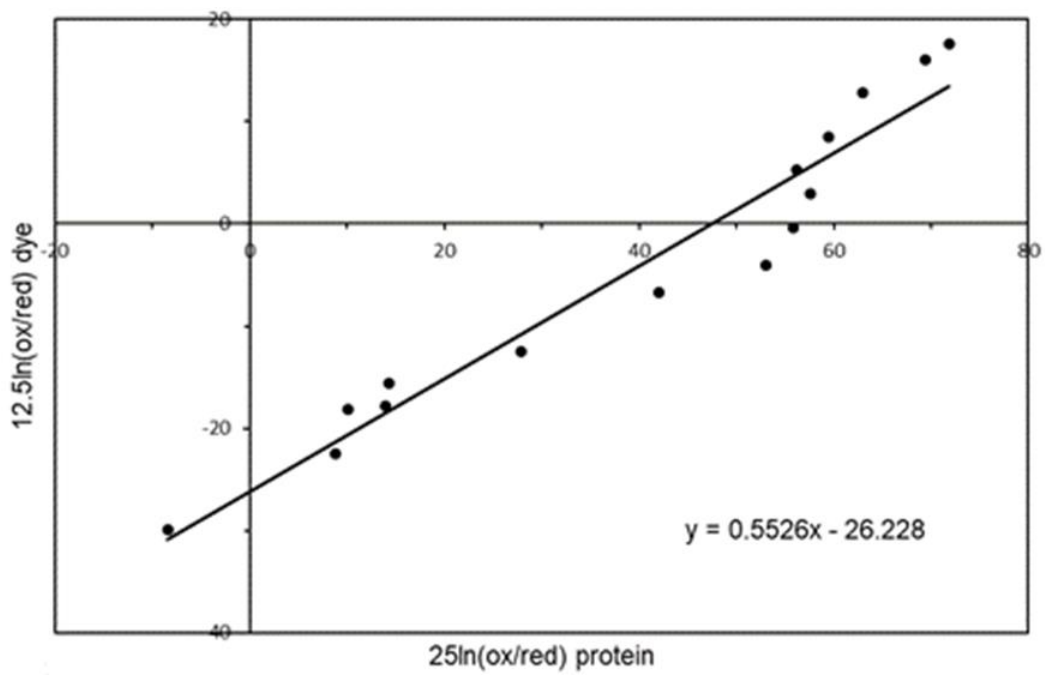

Figure 25. A plot of log(oxidized/reduced) protein versus log(oxidized/reduced) dye.

After each addition of reductant, the ratio of (oxidized/reduced) dye and (oxidized/reduced) protein was determined using the wavelengths fro each component (410 nm and 665 nm for the protein and dye, respectively).

$$\text{oxidized/reduced} = (A - A_{min}) / (A_{max} - A)$$

where A_{max} is the absorbance of the oxidized form, A_{min} is the absorbance of the reduced form and A is the absorbance of each spectrum. The Nernst concentrations for the protein (x) and dye (y) were calculated as shown below. RT/nF is equal to 12.5 for dye and 25 for protein; (R = the gas constant (8.314 J $K^{-1}mol^{-1}$); T = the temperature (25 °C), F = Faraday's constant (96,485 J V^{-1} mol^{-1}); n = number of electrons for reduction of the protein (1 electron) and dye (2 electrons).

$$x = 25 \ln ((A - A_{min}) / (A_{max} - A))$$

$$y = 12.5 \ln ((A - A_{min}) / (A_{max} - A))$$

A plot of y versus x gives a straight line with y intercept equal to the shift in midpoint potential between the protein and the dye (Maklashina & Cecchini, 2020) .

$$E_m \text{ (protein)} = E_m \text{ (dye)} - \text{y-intercept}$$

$$E_m \text{ (protein)} = -4 - (-26.228) = +22.2 \text{ Mv}$$

Rubredoxins from different organisms have different redox potentials ranging from − 100 to +100 mV (vs. SHE) (− 300 to − 100 mV vs. Ag/AgCl) (Gilep et al., 2022) and the redox potential of RubB from *Mycobacterium tuberculosis* has been determined to be –264 mV vs. Ag/AgCl (–67 mV vs SHE) (Sushko et al., 2021). To accurately calculate the redox potential, the protein and dye should have close redox potentials, and the protein and dye reductions should occur at the same rate. However, in this case, the protein was completely reduced before the dye indicating that the difference in their redox potentials does not fall within the recommended 30 mV and the value calculated (+22.2 mV) is an approximation.

CHAPTER 4: CONCLUSION

Bioinformatics analysis showed that the Rv1590 gene is conserved in actinobacteria, and sequence analysis of 100 homologs of the protein encoded by this gene identified 21 residues conserved. The protein is considered a rubredoxin with three cysteines and one histidine acting as metal ligands. Sequence alignment with rubredoxins having solved crystal structures identified key conserved residues, including hydrophobic residues and the three cysteines. The hydrophobic residues form a hydrophobic core that maintains the protein structure and stability. AlphaFold predicts the structure of the protein to belong to the rubredoxin fold with an antiparallel beta-sheet composed of three beta strands.

The Rv1590 gene was expressed in *E. coli,* and the protein encoded by this gene was purified with the SUMO tag. The purified tagged protein had an intense brown color due to the ferric ion confirmed by UV-vis spectroscopy absorption band at 410 nm. However, after cleavage of the SUMO tag, the protein becomes colors due to the loss of ferric ions, indicating that the protein may be unstable on its own. Within the native organism, it may exist bound to other proteins such as Rv1591. Attempts to reconstitute the apoprotein with ferric ions were unsuccessful. However, cobalt and ferrous ion were incorporated into the protein though the amount of inserted ions was not determined.

The CD spectroscopy showed high content of random coils in the protein's secondary structure. Random coils/ unfolded protein may be due to low stability at the experimental temperature (25 °C), unfavorable buffer conditions or the absence of metal ion in the active site. Therefore, he temperature at which the protein is stable and fully folded should be determined and the secondary structure experiment done with the metal-

bound protein atfavorable buffer conditions. Rv1590 was confirmed to be redox active, and the redox potential estimated to be +22.2 mV. However, a more accurate determination of the protein's redox potential is needed.

REFERENCES

Adman, E. T., Sieker, L. C., & Jensen, L. H. (1991). Structure of rubredoxin from Desulfovibrio vulgaris at 1.5 A resolution. *Journal of Molecular Biology*, *217*(2), 337–352. https://doi.org/10.1016/0022-2836(91)90547-j

Archer, M., Carvalho, A. L., Teixeira, S., Moura, I., Moura, J. J. G., Rusnak, F., & Romão, M. J. (1999). Structural studies by X-ray diffraction on metal substituted desulforedoxin, a rubredoxin-type protein. *Protein Science*, *8*(7), 1536–1545. https://doi.org/10.1110/ps.8.7.1536

Barry, C. E., Lee, R. E., Mdluli, K., Sampson, A. E., Schroeder, B. G., Slayden, R. A., & Yuan, Y. (1998). Mycolic acids: structure, biosynthesis and physiological functions. *Progress in Lipid Research*, *37*(2–3), 143–179. https://doi.org/10.1016/S0163-7827(98)00008-3

Berkovitch, F., Nicolet, Y., Wan, J. T., Jarrett, J. T., & Drennan, C. L. (2004). Crystal Structure of Biotin Synthase, an *S* -Adenosylmethionine-Dependent Radical Enzyme. *Science*, *303*(5654), 76–79. https://doi.org/10.1126/science.1088493

Birch, O. M., Fuhrmann, M., & Shaw, N. M. (1995). Biotin Synthase from Escherichiacoli, an Investigation of the Low Molecular Weight and Protein Components Required for Activity inVitro. *Journal of Biological Chemistry*, *270*(32), 19158–19165. https://doi.org/10.1074/jbc.270.32.19158

Buchko, G. W., Hewitt, S. N., Napuli, A. J., van Voorhis, W. C., & Myler, P. J. (2011). Solution-state NMR structure and biophysical characterization of zinc-substituted rubredoxin B (Rv3250c) from *Mycobacterium tuberculosis*. *Acta Crystallographica Section F Structural Biology and Crystallization Communications*, *67*(9), 1148–1153. https://doi.org/10.1107/S1744309111008189

Cammack, R. (2013). Iron-Sulfur Proteins. In *Encyclopedia of Biological Chemistry: Second Edition* (pp. 657–664). Elsevier Inc. https://doi.org/10.1016/B978-0-12-378630-2.00222-X

Casalena, D., Nag, P. P., Park, S., Wilson, D., Edwankar, R., Johnston, S., Le, H., Schilling, R., Bittker, J. A., Dandapani, S., Munoz, B., Dai, R., Finzel, B. C., Schnappinger, D., Aldrich, C., Schreiber, S. L., & Palmer, M. (2010). *Discovery of small molecule probe that shows anti-tubercular activity via Mtb bioA (DAPA synthase) enzyme inhibition*.

Chen, J. C., & Mortenson, L. E. (1992). Two open reading frames (ORFs) identified near the hydrogenase structural genes in Azotobacter vinelandii, the first ORF may encode for a polypeptide similar to rubredoxins. *Biochimica et Biophysica Acta (BBA) - Gene Structure and Expression*, *1131*(1), 122–124. https://doi.org/10.1016/0167-4781(92)90111-C

Choi-Rhee, E., & Cronan, J. E. (2005). Biotin Synthase Is Catalytic In Vivo, but Catalysis Engenders Destruction of the Protein. *Chemistry & Biology*, *12*(4), 461–468. https://doi.org/10.1016/j.chembiol.2005.02.006

Clark, W. M., Cohen, B., & Gibbs, H. D. (1925). Studies on Oxidation-Reduction: VIII. Methylene Blue. *Public Health Reports (1896-1970)*, *40*(23), 1131. https://doi.org/10.2307/4577559

Cramer, J. (2018). *(S)-Adenosyl-L-methionine and the Enzymes That Use it: Inhibition, Mutagenesis and Kinetic Studies from the Biotin Biosynthesis and Methionine Salvage Pathways*. University of Hawaii at Manoa.

Cramer, J. D., & Jarrett, J. T. (2018). Purification, Characterization, and Biochemical Assays of Biotin Synthase From Escherichia coli. *Methods in Enzymology*, *606*, 363–388. https://doi.org/10.1016/bs.mie.2018.06.003

Cronan, J. E., & Lin, S. (2011). Synthesis of the α,ω-dicarboxylic acid precursor of biotin by the canonical fatty acid biosynthetic pathway. *Current Opinion in Chemical Biology*, *15*(3), 407–413. https://doi.org/10.1016/j.cbpa.2011.03.001

Dauter, Z., Wilson, K. S., Sieker, L. C., Moulis, J. M., & Meyer, J. (1996). Zinc- and iron-rubredoxins from Clostridium pasteurianum at atomic resolution: a high-precision model of a ZnS4 coordination unit in a protein. *Proceedings of the National Academy of Sciences of the United States of America*, *93*(17), 8836–8840. https://doi.org/10.1073/pnas.93.17.8836

DeJesus, M. A., Gerrick, E. R., Xu, W., Park, S. W., Long, J. E., Boutte, C. C., Rubin, E. J., Schnappinger, D., Ehrt, S., Fortune, S. M., Sassetti, C. M., & Ioerger, T. R. (2017). Comprehensive Essentiality Analysis of the Mycobacterium tuberculosis Genome via Saturating Transposon Mutagenesis. *MBio*, *8*(1). https://doi.org/10.1128/mBio.02133-16

EATON, W. A., & LOVENBERG, W. (1973). The Iron-Sulfur Complex in Rubredoxin. In *Molecular Properties* (pp. 131–162). Elsevier. https://doi.org/10.1016/B978-0-12-456002-4.50009-5

Farrar, C. E., Siu, K. K. W., Howell, P. L., & Jarrett, J. T. (2010). Biotin Synthase Exhibits Burst Kinetics and Multiple Turnovers in the Absence of Inhibition by Products and Product-Related Biomolecules. *Biochemistry*, *49*(46), 9985–9996. https://doi.org/10.1021/bi101023c

Fenn, J. B., Mann, M., Meng, C. K., Wong, S. F., & Whitehouse, C. M. (1989). Electrospray Ionization for Mass Spectrometry of Large Biomolecules. *Science*, *246*(4926), 64–71. https://doi.org/10.1126/science.2675315

Ferguson, L. A., & Rhoads, J. (2009). Multidrug-resistant and extensively drug-resistant tuberculosis: The new face of an old disease. *Journal of the American Academy of Nurse Practitioners*, *21*(11), 603–609. https://doi.org/10.1111/j.1745-7599.2009.00458.x

Finkenwirth, F., Kirsch, F., & Eitinger, T. (2013). Solitary BioY Proteins Mediate Biotin Transport into Recombinant Escherichia coli. *Journal of Bacteriology*, *195*(18), 4105–4111. https://doi.org/10.1128/JB.00350-13

Fugate, C. J., & Jarrett, J. T. (2012). Biotin synthase: Insights into radical-mediated carbon–sulfur bond formation. *Biochimica et Biophysica Acta (BBA) - Proteins and Proteomics*, *1824*(11), 1213–1222. https://doi.org/10.1016/j.bbapap.2012.01.010

Gámiz-Hernández, A. P., Galstyan, A. S., & Knapp, E.-W. (2009). Understanding Rubredoxin Redox Potentials: Role of H-Bonds on Model Complexes. *Journal of Chemical Theory and Computation*, *5*(10), 2898–2908. https://doi.org/10.1021/ct900328c

Gilep, A., Kuzikov, A., Sushko, T., Grabovec, I., Masamrekh, R., Sigolaeva, L. v., Pergushov, D. v., Schacher, F. H., Strushkevich, N., & Shumyantseva, V. v. (2022a). Electrochemical characterization of mutant forms of rubredoxin B from Mycobacterium tuberculosis. *Biochimica et Biophysica Acta (BBA) - Proteins and Proteomics*, *1870*(1), 140734. https://doi.org/10.1016/j.bbapap.2021.140734

Gilep, A., Kuzikov, A., Sushko, T., Grabovec, I., Masamrekh, R., Sigolaeva, L. v., Pergushov, D. v., Schacher, F. H., Strushkevich, N., & Shumyantseva, V. v. (2022b). Electrochemical characterization of mutant forms of rubredoxin B from Mycobacterium tuberculosis. *Biochimica et Biophysica Acta (BBA) - Proteins and Proteomics*, *1870*(1), 140734. https://doi.org/10.1016/j.bbapap.2021.140734

Gomes, C. M., Silva, G., Oliveira, S., LeGall, J., Liu, M.-Y., Xavier, A. v., Rodrigues-Pousada, C., & Teixeira, M. (1997). Studies on the Redox Centers of the Terminal Oxidase fromDesulfovibrio gigas and Evidence for Its Interaction with Rubredoxin. *Journal of Biological Chemistry*, *272*(36), 22502–22508. https://doi.org/10.1074/jbc.272.36.22502

Greenfield, N. J. (2006). Using circular dichroism spectra to estimate protein secondary structure. *Nature Protocols*, *1*(6), 2876–2890. https://doi.org/10.1038/nprot.2006.202

Gu, S., Chen, J., Dobos, K. M., Bradbury, E. M., Belisle, J. T., & Chen, X. (2003). Comprehensive proteomic profiling of the membrane constituents of a Mycobacterium tuberculosis strain. *Molecular & Cellular Proteomics : MCP*, *2*(12), 1284–1296. https://doi.org/10.1074/mcp.M300060-MCP200

Guianvarc'h, D., Florentin, D., Bui, B. T. S., Nunzi, F., & Marquet, A. (1997). Biotin Synthase, a New Member of the Family of Enzymes Which Uses S-Adenosylmethionine as a Source of Deoxyadenosyl Radical. *Biochemical and Biophysical Research Communications*, *236*(2), 402–406. https://doi.org/10.1006/bbrc.1997.6952

Günther, G. (2014). Multidrug-resistant and extensively drug-resistant tuberculosis: a review of current concepts and future challenges. *Clinical Medicine*, *14*(3), 279–285. https://doi.org/10.7861/clinmedicine.14-3-279

Gupta, N., Bonomi, F., Kurtz, D. M., Ravi, N., Wang, D. L., & Huynh, B. H. (1995). Recombinant Desulfovibrio vulgaris rubrerythrin. Isolation and characterization of the diiron domain. *Biochemistry*, *34*(10), 3310–3318. https://doi.org/10.1021/bi00010a021

Hagelueken, G., Wiehlmann, L., Adams, T. M., Kolmar, H., Heinz, D. W., Tümmler, B., & Schubert, W.-D. (2007). Crystal structure of the electron transfer complex rubredoxin–rubredoxin reductase of *Pseudomonas aeruginosa*. *Proceedings of the National Academy of Sciences*, *104*(30), 12276–12281. https://doi.org/10.1073/pnas.0702919104

Haspel, G., Ehrt, S., & Hillen, W. (1995). Two genes encoding proteins with similarities to rubredoxin and rubredoxin reductase are required for conversion of dodecane to lauric acid in Acinetobacter calcoaceticus ADP1. *Microbiology*, *141*(6), 1425–1432. https://doi.org/10.1099/13500872-141-6-1425

Hausinger, R. P. (1990). Mechanisms of metal ion incorporation into metalloproteins. *BioFactors (Oxford, England)*, *2*(3), 179–184.

Hebbeln, P., Rodionov, D. A., Alfandega, A., & Eitinger, T. (2007). Biotin uptake in prokaryotes by solute transporters with an optional ATP-binding cassette-containing module. *Proceedings of the National Academy of Sciences*, *104*(8), 2909–2914. https://doi.org/10.1073/pnas.0609905104

Holm, R. H., Kennepohl, P., & Solomon, E. I. (1996). Structural and Functional Aspects of Metal Sites in Biology. *Chemical Reviews*, *96*(7), 2239–2314. https://doi.org/10.1021/cr9500390

Huang, W., Jia, J., Gibson, K. J., Taylor, W. S., Rendina, A. R., Schneider, G., & Lindqvist, Y. (1995). Mechanism of an ATP-Dependent Carboxylase, Dethiobiotin Synthetase, Based on Crystallographic Studies of Complexes with Substrates and a Reaction Intermediate. *Biochemistry*, *34*(35), 10985–10995. https://doi.org/10.1021/bi00035a004

Huet, G., Daffé, M., & Saves, I. (2005). Identification of the *Mycobacterium tuberculosis* SUF Machinery as the Exclusive Mycobacterial System of [Fe-S] Cluster Assembly: Evidence for Its Implication in the Pathogen's Survival. *Journal of Bacteriology*, *187*(17), 6137–6146. https://doi.org/10.1128/JB.187.17.6137-6146.2005

Hughes, J. L., & Krausz, E. (2011). Electronic Spectroscopy. In *Encyclopedia of Inorganic and Bioinorganic Chemistry*. John Wiley & Sons, Ltd. https://doi.org/10.1002/9781119951438.eibc0312

Ifuku, O., Koga, N., Haze, S., Kishimoto, J., & Wachi, Y. (1994). Flavodoxin is Required for Conversion of Dethiobiotin to Biotin in Escherichia coli. *European Journal of Biochemistry*, *224*(1), 173–178. https://doi.org/10.1111/j.1432-1033.1994.tb20009.x

IRVING, H., & WILLIAMS, R. J. P. (1948). Order of Stability of Metal Complexes. *Nature*, *162*(4123), 746–747. https://doi.org/10.1038/162746a0

Jameson, G. N. L., Cosper, M. M., Hernández, H. L., Johnson, M. K., & Huynh, B. H. (2004). Role of the [2Fe−2S] Cluster in Recombinant *Escherichia coli* Biotin Synthase. *Biochemistry*, *43*(7), 2022–2031. https://doi.org/10.1021/bi035666v

Jenney, F. E., & Adams, M. W. (2001). Rubredoxin from Pyrococcus furiosus. *Methods in Enzymology*, *334*, 45–55. https://doi.org/10.1016/s0076-6879(01)34457-9

Jitrapakdee, S., St Maurice, M., Rayment, I., Cleland, W. W., Wallace, J. C., & Attwood, P. V. (2008). Structure, mechanism and regulation of pyruvate carboxylase. *Biochemical Journal*, *413*(3), 369–387. https://doi.org/10.1042/BJ20080709

Joseph, C., Stier, G., O'Brien, R., Politou, A. S., Atkinson, R. A., Bianco, A., Ladbury, J. E., Martin, S. R., & Pastore, A. (2001). A Structural Characterization of the Interactions between Titin Z-Repeats and the α-Actinin C-Terminal Domain. *Biochemistry*, *40*(16), 4957–4965. https://doi.org/10.1021/bi002739r

Jumper, J., Evans, R., Pritzel, A., Green, T., Figurnov, M., Ronneberger, O., Tunyasuvunakool, K., Bates, R., Žídek, A., Potapenko, A., Bridgland, A., Meyer, C., Kohl, S. A. A., Ballard, A. J., Cowie, A., Romera-Paredes, B., Nikolov, S., Jain, R., Adler, J., … Hassabis, D. (2021). Highly accurate protein structure prediction with AlphaFold. *Nature*, *596*(7873), 583–589. https://doi.org/10.1038/s41586-021-03819-2

Kapopoulou, A., Lew, J. M., & Cole, S. T. (2011). The MycoBrowser portal: A comprehensive and manually annotated resource for mycobacterial genomes. *Tuberculosis*, *91*(1), 8–13. https://doi.org/10.1016/j.tube.2010.09.006

Keer, J., Smeulders, M. J., Gray, K. M., & Williams, H. D. (2000). Mutants of Mycobacterium smegmatis impaired in stationary-phase survival The GenBank accession numbers for the sequences determined in this work are: AJ277088 (mutant 272A), AJ277089 (mutant 272E), AJ27790 (mutant 317C), AJ277152 (mutant 492A) and AJ276883 (mutant 3910D). *Microbiology*, *146*(9), 2209–2217. https://doi.org/10.1099/00221287-146-9-2209

Kelly, S., & Price, N. (2000). The Use of Circular Dichroism in the Investigation of Protein Structure and Function. *Current Protein & Peptide Science*, *1*(4), 349–384. https://doi.org/10.2174/1389203003381315

Kim, S.-Y., Lee, B.-S., Shin, S. J., Kim, H.-J., & Park, J.-K. (2008). Differentially expressed genes in Mycobacterium tuberculosis H37Rv under mild acidic and hypoxic conditions. *Journal of Medical Microbiology*, *57*(12), 1473–1480. https://doi.org/10.1099/jmm.0.2008/001545-0

Krätzer, C., Welte, C., Dörner, K., Friedrich, T., & Deppenmeier, U. (2011). Methanoferrodoxin represents a new class of superoxide reductase containing an iron-sulfur cluster. *FEBS Journal*, *278*(3), 442–451. https://doi.org/10.1111/j.1742-4658.2010.07964.x

Kurtz, D. M. (2004). Microbial Detoxification of Superoxide: The Non-Heme Iron Reductive Paradigm for Combating Oxidative Stress. *Accounts of Chemical Research*, *37*(11), 902–908. https://doi.org/10.1021/ar0200091

Lovenberg, W., & Sobel, B. E. (1965). Rubredoxin: a new electron transfer protein from Clostridium pasteurianum. *Proceedings of the National Academy of Sciences*, *54*(1), 193–199. https://doi.org/10.1073/pnas.54.1.193

Ludwig Ringlstetter aus Straubing, S. (2010). *Identification of the biotin transporter in Escherichia coli, biotinylation of histones in Saccharomyces cerevisiae and analysis of biotin sensing in Saccharomyces cerevisiae Dissertation*.

Maklashina, E., & Cecchini, G. (2020). Determination of Flavin Potential in Proteins by Xanthine/Xanthine Oxidase Method. *BIO-PROTOCOL*, *10*(7). https://doi.org/10.21769/bioprotoc.3571

Malakhov, M. P., Mattern, M. R., Malakhova, O. A., Drinker, M., Weeks, S. D., & Butt, T. R. (2004). SUMO fusions and SUMO-specific protease for efficient expression and purification of proteins. *Journal of Structural and Functional Genomics*, *5*(1/2), 75–86. https://doi.org/10.1023/B:JSFG.0000029237.70316.52

Marblestone, J. G. (2006). Comparison of SUMO fusion technology with traditional gene fusion systems: Enhanced expression and solubility with SUMO. *Protein Science*, *15*(1), 182–189. https://doi.org/10.1110/ps.051812706

May, S. W., & Kuo, J.-Y. (1978). Preparation and properties of cobalt(II) rubredoxin. *Biochemistry*, *17*(16), 3333–3338. https://doi.org/10.1021/bi00609a025

Mayhew, S. G., & Massey, V. (1973). Studies on the kinetics and mechanism of reduction of flavodoxin from Peptostreptococcus elsdenii by sodium dithionite. *Biochimica et Biophysica Acta (BBA) - Enzymology*, *315*(1), 181–190. https://doi.org/10.1016/0005-2744(73)90141-1

Meyer, J., & Moulis, J.-M. (2006). Rubredoxin. In *Handbook of Metalloproteins*. John Wiley & Sons, Ltd. https://doi.org/10.1002/0470028637.met135

Meyer, T. E., Przysiecki, C. T., Watkins, J. A., Bhattacharyya, A., Simondsen, R. P., Cusanovich, M. A., & Tollin, G. (1983). Correlation between rate constant for reduction and redox potential as a basis for systematic investigation of reaction mechanisms of electron transfer proteins. *Proceedings of the National Academy of Sciences*, *80*(22), 6740–6744. https://doi.org/10.1073/pnas.80.22.6740

Moura, I., Moura, J. J. G., Santos, M. H., Xavier, A. V., & le Gall, J. (1979). Redox studies on rubredoxins from sulphate and sulphur reducing bacteria. *FEBS Letters*, *107*(2), 419–421. https://doi.org/10.1016/0014-5793(79)80421-4

Moura, I., Teixeira, M., Moura, J. J. G., & LeGall, J. (1991). Spectroscopic studies of cobalt and nickel substituted rubredoxin and desulforedoxin. *Journal of Inorganic Biochemistry*, *44*(2), 127–139. https://doi.org/10.1016/0162-0134(91)84025-5

Ohlrogge, J., & Browse, J. (1995). Lipid biosynthesis. *The Plant Cell*, *7*(7), 957–970. https://doi.org/10.1105/tpc.7.7.957

Perkampus, H.-H. (1992). *UV-VIS Spectroscopy and Its Applications*. Springer Berlin Heidelberg. https://doi.org/10.1007/978-3-642-77477-5

Perry, A., Tambyrajah, W., Grossmann, J. G., Lian, L.-Y., & Scrutton, N. S. (2004). Solution structure of the two-iron rubredoxin of Pseudomonas oleovorans determined by NMR spectroscopy and solution X-ray scattering and interactions with rubredoxin reductase. *Biochemistry*, *43*(11), 3167–3182. https://doi.org/10.1021/bi035817u

Peterson, J. A., & Coon, M. J. (1968). Enzymatic ω-Oxidation. *Journal of Biological Chemistry*, *243*(2), 329–334. https://doi.org/10.1016/S0021-9258(18)99296-3

Ragsdale, S. W., Ljungdahl, L. G., & DerVartanian, D. v. (1983). Isolation of carbon monoxide dehydrogenase from Acetobacterium woodii and comparison of its properties with those of the Clostridium thermoaceticum enzyme. *Journal of Bacteriology*, *155*(3), 1224–1237. https://doi.org/10.1128/jb.155.3.1224-1237.1983

Rengarajan, J., Bloom, B. R., & Rubin, E. J. (2005). Genome-wide requirements for *Mycobacterium tuberculosis* adaptation and survival in macrophages. *Proceedings of the National Academy of Sciences*, *102*(23), 8327–8332. https://doi.org/10.1073/pnas.0503272102

Roth, K. S. (1981). Biotin in clinical medicine—a review. *The American Journal of Clinical Nutrition*, *34*(9), 1967–1974. https://doi.org/10.1093/ajcn/34.9.1967

Russell DW, S. J. (2001). *Molecular cloning: a laboratory manual*.

Said, H. M. (2009). Cell and Molecular Aspects of Human Intestinal Biotin Absorption. *The Journal of Nutrition*, *139*(1), 158–162. https://doi.org/10.3945/jn.108.092023

Salaemae, W., Azhar, A., Booker, G. W., & Polyak, S. W. (2011). Biotin biosynthesis in Mycobacterium tuberculosis: physiology, biochemistry and molecular intervention. *Protein & Cell*, *2*(9), 691–695. https://doi.org/10.1007/s13238-011-1100-8

Sassetti, C. M., Boyd, D. H., & Rubin, E. J. (2001). Comprehensive identification of conditionally essential genes in mycobacteria. *Proceedings of the National Academy of Sciences*, *98*(22), 12712–12717. https://doi.org/10.1073/pnas.231275498

Sassetti, C. M., Boyd, D. H., & Rubin, E. J. (2003). Genes required for mycobacterial growth defined by high density mutagenesis. *Molecular Microbiology*, *48*(1), 77–84. https://doi.org/10.1046/j.1365-2958.2003.03425.x

Sassetti, C. M., & Rubin, E. J. (2003). Genetic requirements for mycobacterial survival during infection. *Proceedings of the National Academy of Sciences of the United States of America*, *100*(22), 12989–12994. https://doi.org/10.1073/pnas.2134250100

Shiloh, M. U. (2016). Mechanisms of mycobacterial transmission: how does *Mycobacterium tuberculosis* enter and escape from the human host. *Future Microbiology*, *11*(12), 1503–1506. https://doi.org/10.2217/fmb-2016-0185

Sieker, L. C., Stenkamp, R. E., Jensen, L. H., Prickril, B., & LeGall, J. (1986). Structure of rubredoxin from the bacterium *Desulfovibrio desulfuricans*. *FEBS Letters*, *208*(1), 73–76. https://doi.org/10.1016/0014-5793(86)81535-6

Sieker, L. C., Stenkamp, R. E., & LeGall, J. (1994). Rubredoxin in crystalline state. *Methods in Enzymology*, *243*, 203–216. https://doi.org/10.1016/0076-6879(94)43016-0

Sievers, F., Wilm, A., Dineen, D., Gibson, T. J., Karplus, K., Li, W., Lopez, R., McWilliam, H., Remmert, M., Söding, J., Thompson, J. D., & Higgins, D. G. (2011). Fast, scalable generation of high-quality protein multiple sequence alignments using Clustal Omega. *Molecular Systems Biology*, *7*(1), 539. https://doi.org/10.1038/msb.2011.75

Stillman, M. (2007). Biological Inorganic Chemistry. Structure and Reactivity. Edited by Ivano Bertini, Harry B. Gray, Edward I. Stiefel and Joan S. Valentine. *Angewandte Chemie International Edition*, *46*(46), 8741–8742. https://doi.org/10.1002/anie.200785504

Sushko, T., Kavaleuski, A., Grabovec, I., Kavaleuskaya, A., Vakhrameev, D., Bukhdruker, S., Marin, E., Kuzikov, A., Masamrekh, R., Shumyantseva, V., Tsumoto, K., Borshchevskiy, V., Gilep, A., & Strushkevich, N. (2021a). A new twist of rubredoxin function in M. tuberculosis. *Bioorganic Chemistry*, *109*, 104721. https://doi.org/10.1016/j.bioorg.2021.104721

Sushko, T., Kavaleuski, A., Grabovec, I., Kavaleuskaya, A., Vakhrameev, D., Bukhdruker, S., Marin, E., Kuzikov, A., Masamrekh, R., Shumyantseva, V., Tsumoto, K., Borshchevskiy, V., Gilep, A., & Strushkevich, N. (2021b). A new twist of rubredoxin function in M. tuberculosis. *Bioorganic Chemistry*, *109*, 104721. https://doi.org/10.1016/j.bioorg.2021.104721

Swartz, P. D., & Ichiye, T. (1997). Protein contributions to redox potentials of homologous rubredoxins: an energy minimization study. *Biophysical Journal*, *73*(5), 2733–2741. https://doi.org/10.1016/S0006-3495(97)78302-4

Taylor, K. P., Parks, B. A., Kurtz, D. M., & Amster, J. I. (2001). Analysis of metal incorporation during overexpression of Clostridium pasteurianum rubredoxin by electrospray FTICR mass spectrometry. *JBIC Journal of Biological Inorganic Chemistry*, *6*(2), 201–206. https://doi.org/10.1007/s007750000197

Tong, L. (2013). Structure and function of biotin-dependent carboxylases. *Cellular and Molecular Life Sciences*, *70*(5), 863–891. https://doi.org/10.1007/s00018-012-1096-0

Tse Sum Bui, B., Lotierzo, M., Escalettes, F., Florentin, D., & Marquet, A. (2004). Further Investigation on the Turnover of *Escherichia coli* Biotin Synthase with Dethiobiotin and 9-Mercaptodethiobiotin as Substrates. *Biochemistry*, *43*(51), 16432–16441. https://doi.org/10.1021/bi048040t

Ugulava, N. B., Gibney, B. R., & Jarrett, J. T. (2000). Iron-sulfur cluster interconversions in biotin synthase: dissociation and reassociation of iron during conversion of [2Fe-2S] to [4Fe-4S] clusters. *Biochemistry*, *39*(17), 5206–5214. https://doi.org/10.1021/bi9926227

Ugulava, N. B., Gibney, B. R., & Jarrett, J. T. (2001). Biotin Synthase Contains Two Distinct Iron−Sulfur Cluster Binding Sites: Chemical and Spectroelectrochemical Analysis of Iron−Sulfur Cluster Interconversions. *Biochemistry*, *40*(28), 8343–8351. https://doi.org/10.1021/bi0104625

Ugulava, N. B., Sacanell, C. J., & Jarrett, J. T. (2001). Spectroscopic changes during a single turnover of biotin synthase: destruction of a [2Fe-2S] cluster accompanies sulfur insertion. *Biochemistry*, *40*(28), 8352–8358. https://doi.org/10.1021/bi010463x

Vincent Massey. (1991). A SIMPLE METHOD FOR THE DETERMINATION OF REDOX POTENTIALS. In *Flavins and Flavoproteins 1990* (pp. 59–66). De Gruyter. https://doi.org/10.1515/9783110855425-012

Wan, J. T., & Jarrett, J. T. (2002). Electron acceptor specificity of ferredoxin (flavodoxin):NADP+ oxidoreductase from Escherichia coli. *Archives of Biochemistry and Biophysics*, *406*(1), 116–126. https://doi.org/10.1016/S0003-9861(02)00421-6

Wastl, J., Sticht, H., Maier, U. G., Rösch, P., & Hoffmann, S. (2000). Identification and characterization of a eukaryotically encoded rubredoxin in a cryptomonad alga. *FEBS Letters*, *471*(2–3), 191–196. https://doi.org/10.1016/s0014-5793(00)01399-5

Weeks, S. D., Drinker, M., & Loll, P. J. (2007). Ligation independent cloning vectors for expression of SUMO fusions. *Protein Expression and Purification*, *53*(1), 40–50. https://doi.org/10.1016/j.pep.2006.12.006

Wilschefski, S., & Baxter, M. (2019). Inductively Coupled Plasma Mass Spectrometry: Introduction to Analytical Aspects. *Clinical Biochemist Reviews*, *40*(3), 115–133. https://doi.org/10.33176/AACB-19-00024

Yoon, K.-S., Hille, R., Hemann, C., & Tabita, F. R. (1999). Rubredoxin from the Green Sulfur Bacterium Chlorobium tepidum Functions as an Electron Acceptor for Pyruvate Ferredoxin Oxidoreductase. *Journal of Biological Chemistry*, *274*(42), 29772–29778. https://doi.org/10.1074/jbc.274.42.29772